Special classes of terrestrial gamma-ray flashes from RHESSI

D. M. Smith[1], N. A. Kelley[2], P. Buzbee[3], A. Infanger[4], M. Splitt[5], R. H. Holzworth[6], J. R. Dwyer[7]

[1]Santa Cruz Institute for Particle Physics and Physics Department, University of California, Santa Cruz, Santa Cruz, California, USA.
[2]Cruise Automation, San Francisco, California, USA.
[3]Google Inc., Mountain View, California, USA.
[4]Institute for Computational and Mathematical Engineering, Stanford University, Palo Alto, California, USA.
[5]College of Aeronautics, Florida Institute of Technology, Melbourne, Florida, USA.
[6]Department of Earth and Space Sciences, University of Washington, Seattle, Washington, USA.
[7]Institute for the Study of Earth, Oceans, and Space, University of New Hampshire, Durham, New Hampshire, USA.

Key Points:

- The Comptonized "tail" of a TGF can be used to find its luminosity independent of its original beam width.
- Many TGFs of duration more than a few hundred microseconds probably include detection of the upward-going electron beam.
- Particularly short TGFs tend to occur more often over open ocean than longer TGFs.

Corresponding author: David M. Smith, `dsmith8@ucsc.edu`

Abstract

We report on three classes of terrestrial gamma-ray flashes (TGFs) from the Reuven Ramaty High-Energy Solar Spectroscopic Imager (RHESSI) satellite. The first class drives the detectors into paralysis, being observed usually through a few counts on the rising edge and the later tail of Comptonized photons. These events – and any bright TGF – reveal their true luminosity more clearly via their Compton tail than via the main peak, since the former is unaffected by the unknown beaming pattern of the unscattered radiation, and Comptonization mostly isotropizes the flux. This technique could be applied to TGFs from any mission. The second class is more than usually bright and long in duration. When the magnetic field at the conjugate point is stronger than at the nearby footpoint, we find that 4 out of 11 such events show a significant signal at the time expected for a relativistic electron beam to make a round trip to the opposite footpoint and back. We conclude that a large fraction of TGFs lasting more than a few hundred microseconds may include counts due to the upward-moving secondary particle beam ejected from the atmosphere. Finally, using a new search algorithm to find short TGFs in RHESSI, we see that these tend to occur more often over the oceans than land, relative to longer-duration events. In the feedback model of TGF production, this suggests a higher thunderstorm potential, since more feedback per avalanche implies fewer "generations" of avalanches needed to complete the TGF discharge.

1 Introduction

Terrestrial gamma-ray flashes (TGFs) are bright, millisecond and sub-millisecond bursts of gamma rays originating from thunderstorms. They were first seen by the Burst and Transient Source Experiment (BATSE) aboard the *Compton Gamma-ray Observatory (CGRO)* in 1994 (Fishman et al.,). Since then, four other satellites have observed greater numbers of TGFs: the Reuven Ramaty High Energy Spectroscopic Imager (RHESSI) (Smith et al.,), the Fermi Gamma-ray Space Telescope (Briggs et al.,), the Astrorivelatore Gamma a Immagini Leggero (AGILE) (Marisaldi et al.,), and most recently the Atmosphere-Space Interactions Module (ASIM) module on the International Space Station (Østgaard et al.,).

TGF gamma-rays have energies up to tens of MeV, and the accepted mechanism for explaining their spectrum is relativistic runaway electron avalanches (RREA) (Gurevich et al., ,). Maximal avalanche growth of available fast atmospheric seed electrons is still not enough to account for the intensities of TGFs (Dwyer,), usually thought to be $\sim 10^{17}-10^{18}$ relativistic electrons or gamma-ray photons at the source (Dwyer & Smith, , ,). Two current models may explain the brightness of TGFs. The relativistic feedback model builds on RREA by including both positron and gamma-ray feedback, where positrons, created by pair production, and Compton scattered gamma rays travel to the beginning of the avalanche region and initiate new avalanches (Dwyer,). In the other family of models, the enhanced electric field at the end of stepped leaders in lightning accelerates all free electrons to relativistic energies in a process called cold runaway. This creates a large relativistic seed population to be multiplied during a second stage of acceleration (RREA), thus accounting for the intensity of TGFs. The second stage of acceleration may take place either in a more distant part of the leader field (Moss et al., , , , e.g.) or in the large-scale field of the thunderstorm (Moss et al., ,).

In this paper we present results on three specific classes of TGFs observed with RHESSI, following up on a general survey of RHESSI TGF characteristics (Grefenstette et al.,) and more specialized studies of RHESSI TGF thunderstorm characteristics (Splitt et al.,), geographical distribution and storm phase (Smith et al.,), and limits on gamma-ray luminosity of lightning flashes that don't show a bright TGF (Smith et al.,). First, in Section 2 we discuss events that are so bright that they paralyze RHESSI's electronics, being detectable primarily by the delayed, weaker set of photons that have Compton scattered in Earth's atmosphere, usually multiple times. These Comptonized photons turn out to give a particular advantage in determining the intrinsic brightness of the TGF, since the intensity of the scattered photons is only weakly dependent on the original (and unknown) angular distribution of the original gamma-ray beam.

Next, in Section 3, we identify a small number of events in which the secondary electron beam from the TGF (Dwyer et al., , ,) travels along a magnetic field line to the magnetic conjugate point, reflects there, and returns to the spacecraft. This behavior is predicted to occur when the field is stronger in the conjugate hemisphere. We find that nearly half of TGFs chosen only for their long duration and brightness turn out to have a significant return beam, suggesting that most long and bright TGFs probably include an upward electron component seen at the spacecraft in addition to the primary gamma rays.

Finally, in Section 4, by tuning the parameters of the RHESSI TGF search algorithm, we find a population of TGFs shorter than the original algorithm (Grefenstette et al.,) was capable of finding (the new algorithm is closer to that of Gjesteland et al. ()). These short TGFs are found to be more concentrated in the open ocean than longer ones, a result that holds around the globe.

2 "Paralyzing" TGFs and Compton-tail analysis

2.1 The luminosity distribution of TGFs

To understand how common TGFs are, and further constrain the mechanism of their creation, the distribution of luminosities needs to be known. The differential fluence distribution of TGFs has been found by several authors to be consistent with a power law of index -2.2 to -2.4, using RHESSI and Fermi together (Østgaard et al.,), Fermi alone (Tierney et al.,), and AGILE (Marisaldi et al.,), but it is uncertain whether this distribution continues below the cutoff sensitivity of Fermi's Gamma-ray Burst Monitor, the most sensitive of the instruments with a large data set, or the new ASIM (Østgaard et al.,). The ADELE airborne instrument placed constraints on both the number of full-sized and weak (1% of normal) TGFs from observations at close proximity to lightning (Smith et al.,). Searches for faint TGFs associated with lightning flashes identified by their radio emission have revealed a small number of events (Østgaard et al.,), but the summed gamma-ray emission from lightning is far lower than would be expected if the power law distribution continues much below the sensitivity limit of the current satellites (Smith et al.,). Further analysis of this population of weak events indeed indicates that the power law flattens out at low luminosity (Albrechtsen et al.,).

The empirical power-law distribution of TGFs' observed brightness includes not only the effect of the intrinsic brightness distribution, but also of their distribution with respect to distance from the sub-satellite point, degree of upward beaming, and altitude of production. If some TGFs are occurring at lower altitudes, they could be much brighter; the number of photons observable from space drops by 1/e for each 45 g/cm^2 of intervening atmosphere (Smith et al.,). Gjesteland et al. (), using RHESSI data, found an unusually bright TGF over the Mediterranean sea, produced at an unusually low altitude, implying an unexpectedly high intrinsic brightness. Satellites may also miss or mischaracterize brighter TGFs. BATSE, RHESSI, Fermi, and AGILE were not designed to tolerate very high count rates, and can show significant dead time during TGF observing.

The small number of TGFs at the highest luminosities makes the upper end of the luminosity distribution a relatively unexplored frontier. Mailyan et al. (), by studying individual TGF spectra with Fermi, derived values of up to 10^{19} for the number of relativistic electrons in the brightest TGFs. Better understanding of the bright end of the TGF distribution would offer new opportunities to constrain the physics of their pro-

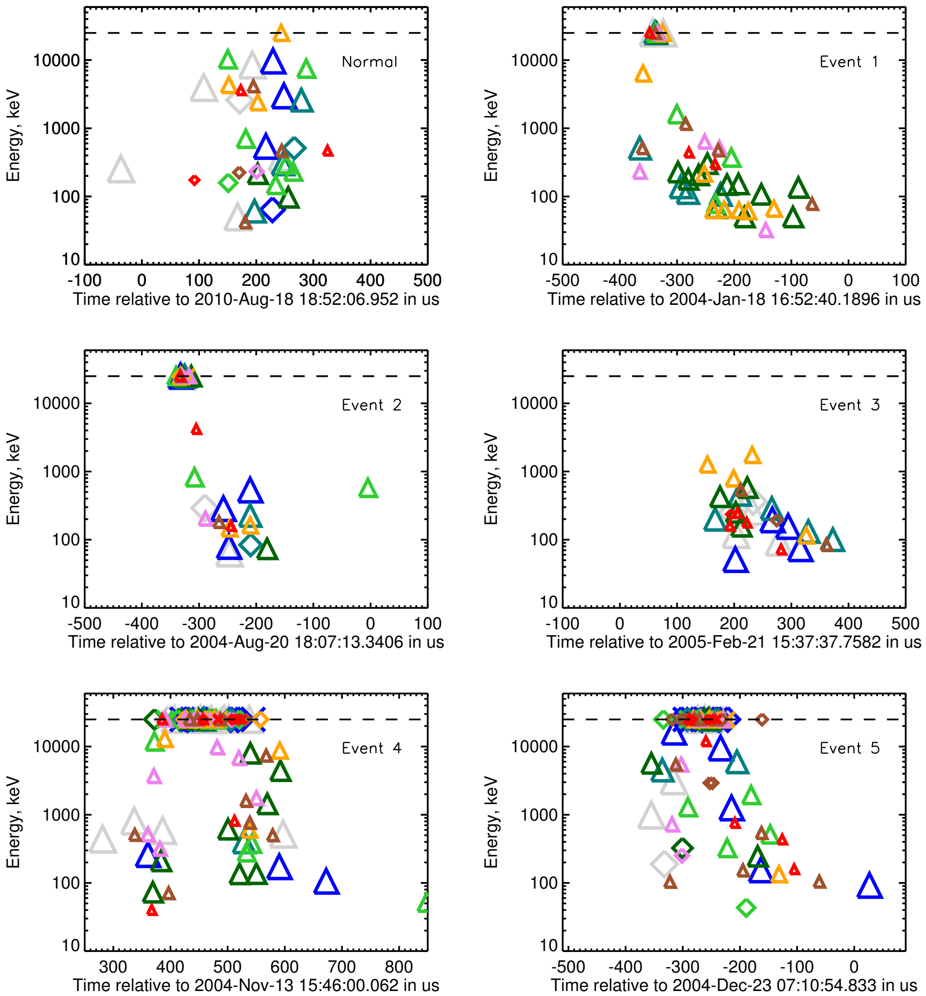

Figure 1. Energy and timing of individual detector counts for six TGFs. Each symbol represents a photon interaction in one of RHESSI's detector segments (see text).

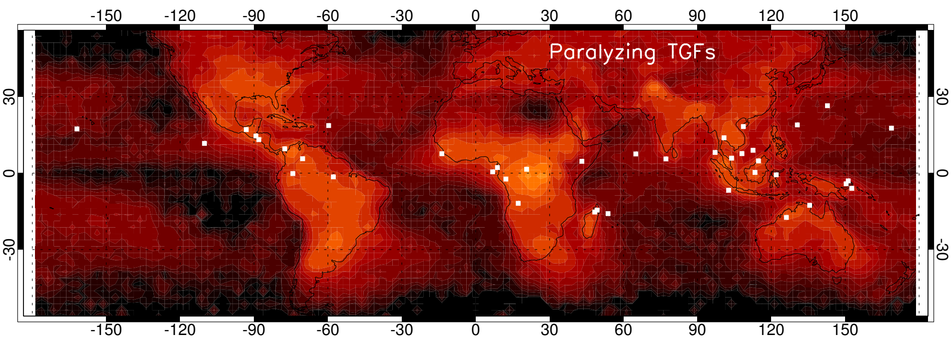

Figure 2. Global distribution of 40 paralyzing TGFs. The background color scale is relative annual flash rate from LIS/OTD gridded lightning climatology data (Cecil et al.,).

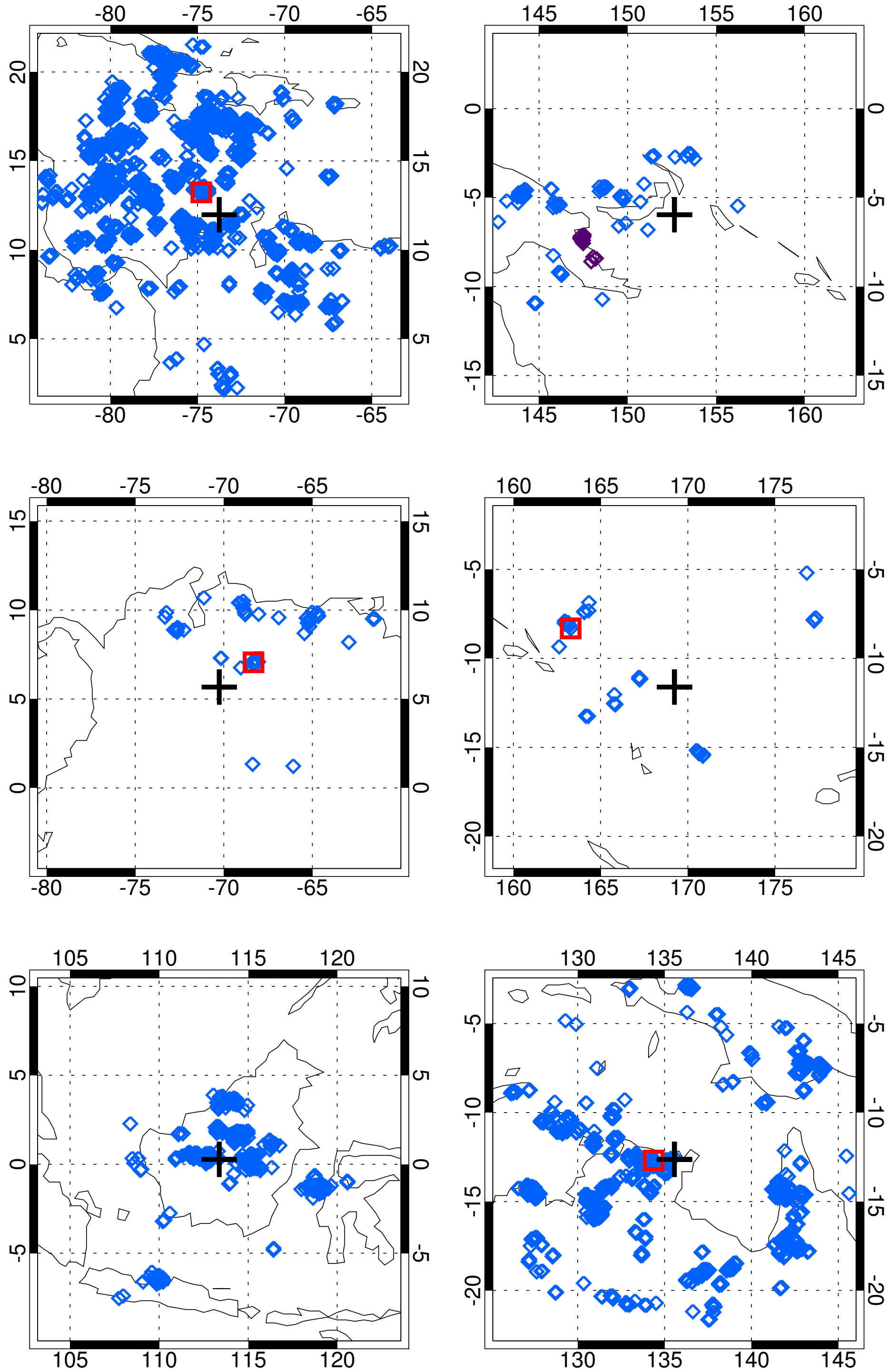

Figure 3. Blue diamonds: WWLLN flashes within ±30 min of the six TGFs shown in Figure 1. Black cross: the subsatellite position of RHESSI. Red squares: flash **associated** with the TGF (within <1 s) when detected by WWLLN. For Event 1 (upper right), the flashes in purple are in the distance range of 550–650 km of the subsatellite point, the range favored by the simulations of a narrow-beam TGF (see section 2.6.1).

Table 1. TGFs discussed in the context of of paralyzing events

Event name	Date	Time (UTC)	RHESSI or *Fermi* Coordinates (lat., E.lon.)	Lightning Coordinates (lat., E.lon.)	Dist. from subsatellite point (km)	Cloudtop altitude (km)[i]	TGF altitude estimate (km)
Cummer 1 (*Fermi*)	2011-Aug-01	02:57:17.409[f]	24.516, −84.963	22.529, −82.160[f]	361		11.8 ± 0.4[h]
Cummer 2 (*Fermi*)	2013-Sep-25	05:25:13	23.709, 84.375	28.342, −86.292[g]	548		11.9 ± 0.9[h]
Lu 1 (RHESSI)	2008-Jul-26	09:38:16.274	36.156, −87.883	not reported	30	14.6	10–13[d]
"Normal" event	2010-Aug-18	18:52:06.952[c]	11.975, −73.752	unknown	unknown		
Event 1 ("bright")	2004-Jan-18	16:52:40.191[c]	−5.964, 152.643	unknown	unknown		
Event 2 ("near")	2004-Aug-20	18:07:13.341[c]	5.671, −70.258	7.062, −68.323[b]	264	14.9	10.3–13.3[e]
Event 3 ("far")	2005-Feb-21	15:37:37.758[c]	−11.611, 169.232	−8.321, 163.286[b]	747	17.6	13–16[e]
Event 4 ("longest")	2004-Nov-13	15:46:00.062[c]	0.273, 113.376	unknown	unknown		
Event 5 ("long")	2004-Dec-23	07:10:54.833[c]	−12.632, 135.569	−12.699, 134.375[b]	130	16.7	12.1–15.1[e]

[a] Coordinates of RHESSI subsatellite point

[b] Coordinates of matching WWLLN stroke

[c] RHESSI gamma-ray arrival time, with clock correction but no light propagation correction

[d] Range is from the position of the upward leader at the time of the TGF to the center of the main positive charge center, according to LMA data

[e] By analogy with the Lu et al. event (keeping the same distance between the IR top and the TGF altitude)

[f] From National Lightning Detection Network data

[g] From Earth Networks Total Lightning Network data

[h] Values derived from ionospheric reflection of LF signals exactly simultaneous with the gamma-ray emission

[i] See Appendix for details on these estimates

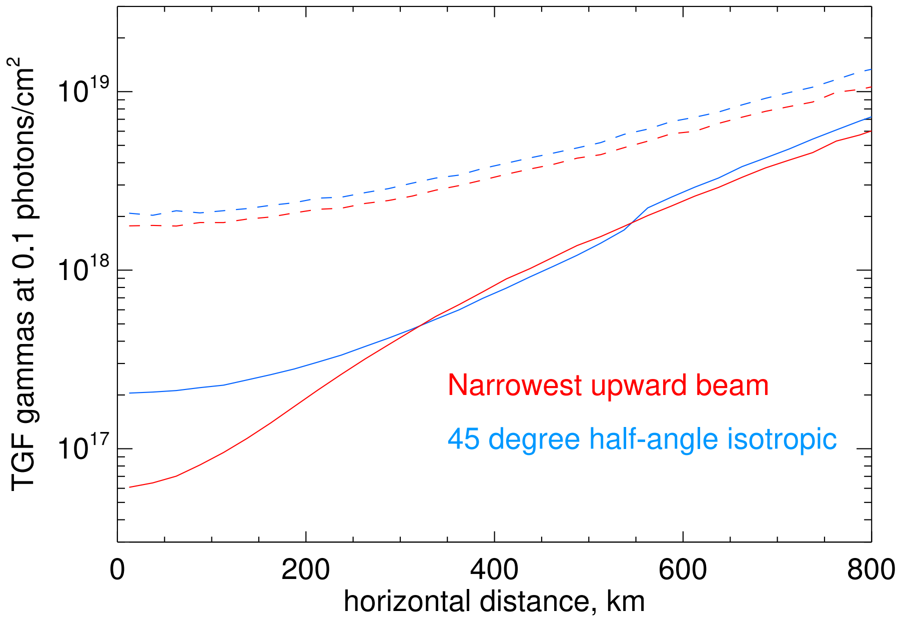

Figure 4. The relative independence of luminosity estimates on TGF beaming when using only the Compton tail. Solid lines: derived luminosity estimates (in total TGF gammas) for 0.1 photons/cm^2 observed fluence at a spacecraft using all TGF gammas. Dashed lines: using photons in the Compton tail only ($> 50\mu$s delay), assuming 0.1 photons/cm^2 in that component.

duction and the potential radiation risk to people in aircraft (Dwyer et al.,). At some point, the available potential energy in the thundercloud charge distribution provides a limit to a TGF's luminosity, but whether TGF physics implies a more modest cutoff is unknown.

In this section we present members of a rare subset of TGFs from RHESSI that show signs of being considerably brighter than the traditional luminosity of $\sim 10^{17} - 10^{18}$ gamma-ray photons (Dwyer & Smith, , e.g.). We demonstrate a new method to estimate the luminosity of these events using only the subset of detected gamma-rays that have been delayed by repeated Compton scattering in Earth's atmosphere. Because these photons have been effectively isotropized, this method has the advantage of removing the dependence of the luminosity calculation on the unknown angular distribution of the gamma-rays when they are produced.

Nemiroff, Bonnell, and Norris () were the first to notice that some TGFs were softer in their later stages, and the interpretation of this phenomenon as due to atmospheric Compton scattering has been discussed by a number of authors (Østgaard et al., , , ,). Babich, Donskoy, and Kutsyk () explored the degree of Comptonization versus source altitude without specific reference to time delays. Celestin and Pasko () showed that some of the shortest TGFs appear consistent with Compton scattering of an instantaneously created photon population.

2.2 RHESSI instrumental effects

The RHESSI satellite was launched in **February** 2002 by NASA to study high-energy solar physics **and decommissioned in August 2018**. The instrument consisted of nine germanium detectors, segmented into thin front segments dedicated to solar x-rays and thicker rear segments for solar gamma-rays (Smith et al.,). The rear segments, which we use for TGF searches in the data, were sensitive from 25 keV–17 MeV and had roughly isotropic sensitivity at MeV energies, **with a total effective area of $\sim 250\mathbf{cm}^2$ for a typical atmospherically Comptonized RREA spectrum**. RHESSI continuously recorded every count with 1 μs timing precision and $\sim$ 1 ms absolute timing knowledge and telemetered those data to the ground, where offline searches for TGFs are performed. Over 3000 TGFs have been detected by the instrument using algorithms developed by our group (Grefenstette et al.,) and by the University of Bergen (Gjesteland et al.,) (see section 4.2).

We recently found a subset of RHESSI TGFs that are so bright that they cause the instrument to be paralyzed, recording no valid counts at all during the peak of the event. This is due primarily to the very aggressive pile-up rejection in RHESSI's detector electronics. When two counts occur in a detector segment within 6 μs, not only is the second count rejected as likely to be contaminated by the tail of the first pulse, but the first pulse is rejected as well (from 6 μs to 9 μs delay, only the second event is rejected, as in a more typical pile-up-rejection circuit). Thus, for as long as counts are coming in quickly enough, no counts at all will be registered in that detector. We will refer to TGFs that appear to contain such an interval as "paralyzing" events.

Simulations of the instrument's physical response with GEANT3 and of its electronics response with a custom code show that it takes a rate of about 3 hits per microsecond in the whole instrument, or about 300 kHz count rate per detector, to produce a complete veto of all counts registered in the rear segments, and about 10 hits per microsecond to veto all counts in both front and rear segments. A "hit" in this context means an interaction between an incoming gamma-ray and a detector segment (the photon might scatter several times in that segment, but these interactions can't be separated and are considered part of the same "hit"). The average number of hits per each photon entering the simulation and interacting with the detectors varies from 1.04 to 1.24 depending on the hardness of the TGF spectrum, which in turn depends on the depth at which the TGF is produced and the distance away from the center of the beam. The number is higher for harder spectra, since the photons are more likely to scatter from one segment or detector to another. A typical RHESSI TGF produces roughly 15–30 hits over a period on the order of 100μs, so normally we are far below the regime of paralysis.

At these very high hit rates, even for a short period, there is also a possibility that several of RHESSI's detectors will experience a preamplifier reset. In RHESSI's pulsed-transistor-reset, charge-sensitive preamplifiers (Landis et al.,), charge accumulated on the feedback capacitor is removed abruptly, with a brief interruption in the detector's operation, when it reaches a certain level. In RHESSI's case the reset occurs when the charge corresponds to what is collected from about 40 MeV of energy deposited in the detector, which, for the very hard TGF spectrum, can correspond to only a handful of photons. The reset lasts for 20–40 μs, depending on the segment, which can represent a significant fraction of the duration of the prompt part of a TGF and/or the early stages of the Compton tail.

False upper-level-discriminator (ULD) events can be created during the reset process and enter the data stream. True ULD events represent energy deposits greater than the maximum measurable on the analog-to-digital conversion energy scale (about 17 MeV for rear segments). In TGFs, ULDs can represent real gamma-rays and are usually kept in our analysis. But false ULDs created by resets in paralyzed events should not be considered as representing real gamma-ray interactions. Thus counting these false ULDs during periods where in-scale gamma-rays are suppressed by paralysis cannot be used as a valid means to estimate the energy deposited in the detectors. Unfortunately, rear segment reset events are not included in the RHESSI data stream, so true and false ULDs cannot be reliably distinguished. We consider a TGF to be "paralyzing" (creating no real counts) when there is an interval **(typically 20–40μs)** containing nothing but reset and/or ULD events.

2.3 Paralyzing vs. normal TGFs

The possibility of this kind of paralysis suggests that there could be a significant population of very short TGFs just above the paralysis threshold that avoid detection by RHESSI by producing very few counts outside the period of paralysis. But assuming that these events have a rise-time comparable to ordinary TGFs, of a few microseconds or more, they should usually produce a count or two before paralysis kicks in. While a normal TGF search wouldn't find this population of events, the stacking analysis we performed on RHESSI data when the spacecraft was passing over lightning would have found their collective signal, and did not (Smith et al.,). We concluded in that paper that a large population of relatively weak, short events cannot exist.

But for bright enough short events, there must be a considerable number of counts delayed by tens of microseconds by Compton scattering in Earth's atmosphere, and these could be detected without paralysis. Of the paralyzing events we have discovered, many have such a bright Compton tail. The rest have a slow enough rise and/or fall out of the paralyzed interval that they can be detected even without a Comptonized, delayed tail.

Figure 1 shows several TGFs as time/energy scatter plots, in which each point represents a single hit on a detector segment. The upper-left plot shows a somewhat brighter than average but otherwise ordinary TGF; the other **five** panels show events with exceptionally bright Compton tails. They are discussed in more detail in the next section. Rear-segment energy deposits are represented by triangles and front-segment deposits by diamonds. There are nine colors, each matched by a symbol size, representing the nine RHESSI detector segments; this feature of the plots is useful only to demonstrate that real TGFs are not dominated by events in one or a small fraction of the detectors (bursts of false events following large cosmic-ray interactions, which can otherwise be mistaken for TGFs, are). Two of the TGFs show no front segment events because they occurred during spacecraft night and front-segment events were temporarily excluded from the telemetry stream, as was sometimes the case when the satellite's memory was filling up. ULD events and front-segment reset events are shown at the upper dashed line, although as mentioned above they represent only a qualitative indication that a large energy deposit has occurred; the size of that deposit cannot be readily estimated. Events below 25 keV have been excluded from the plots. These are most likely to be due to a crosstalk effect from an energy deposit in the opposite segment of the same detector, as discussed in Smith et al. ().

We have found 40 TGFs that clearly appear to be paralyzing, with a comparable number that suggest a nearly-paralyzed interval within the event. These were found by visual inspection of the subset of RHESSI events that include several ULD counts. We believe the paralyzing events to be real TGFs because their geographic distribution (Figure 2) is similar to previously observed RHESSI TGFs, as is the appearance of their energy spectrum in the brief interval before paralysis. We have also found nearby lightning-producing storms using World Wide Lightning Location Network (WWLLN) data for 28 of the 31 paralyzing events for which WWLLN data are available. A match to a storm was defined as at least eight WWLLN flashes within 600 km and $\pm$10 min of the TGF. Figure 2 is similar to previous RHESSI TGF maps (Grefenstette et al., ,), with the population being dominated by the three conventional lightning "chimneys" of the Americas, Africa, and Southeast Asia, with perhaps an extra weighting toward equatorial and coastal regions relative to lightning.

We selected for further discussion four paralyzing events and a fifth event that appears to consist only of a Compton tail, with not only no paralyzing stage, but no un-Comptonized peak at all. The location of the satellite and time of the event are shown for each TGF in Table 1, along with other information discussed below. Figure 3 shows the nearby, contemporaneous lightning activity as seen by WWLLN for these five events and the "normal" TGF presented for comparison in Figure 1.

Event 1 (2004 January 18) is notable for having the brightest Compton tail we have visibly identified, and a very clear display of the short rise phase, short period of paralysis, and extended tail characteristic of the paralyzing events. The paralyzed period in this new class of events (and hence the main peak of the TGF) is nearly always quite short; about 30 μs in this case, which is typical. By contrast, the normal TGF in Figure 1 lasts about 200 μs, which is on the short side of events in the first RHESSI catalog (Grefenstette et al.,) but more typical of events seen in the newer algorithms (see Gjesteland et al. () and section 4 below).

Event 2 is one of a few events that show no counts at all before paralysis occurs, suggesting a rise time of only a few microseconds. This is not unprecedented, Fermi having seen three TGFs with rise times estimated as 7–9 μ s (Foley et al.,). **In general, more recent results have shown that there are more short (10s of μs) TGFs than formerly known; the evidence includes the reanalysis of AGILE data (Marisaldi et al.,) and the new data from ASIM, with its particularly high sensitivity (Østgaard et al.,).** Event 2 is matched to a specific WWLLN sferic, showing that it occurred at a surface distance of 264 km from the satellite footprint. **WWLLN matches are defined throughout this paper as a time difference of < 10 ms between the TGF and the WWLLN sferic. In Smith et al. () we showed that this interval captures more true matches than a requirement of simultaneity within uncertainties. We suggested that these were cases where the sferic and TGF occurred during different parts of the leader ascent. We found that the probability of an accidental association in this interval averaged 3.4×10^{-4}.**

Event 3 is the one that appears to be only a Compton tail, with no primary peak, paralyzing or otherwise. It also matches a specific WWLLN sferic, and is one of the most distant of these direct matches that we have, at 747 km. This makes it quite plausible that only Comptonized photons would be seen, with the direct bremsstrahlung beam missed entirely. This possibility was confirmed as plausible via simulations as discussed below. Unlike the other two events, which were discovered by a visual survey of TGFs with a lot of ULD counts, this event was discovered in a visual survey of TGFs matched to a WWLLN flash. This suggests that there may be more Compton-only events to be found in the overall data set that don't match a WWLLN signal. An event very much like this one was shown by Mailyan et al. () (see their Figure 1, bottom right panel, and their section 3.1) and was also relatively distant (475 km from the Fermi subsatellite point). **They reanalyzed this event in the context of a model assuming a diverging field at a lightning leader tip as well (Mailyan et al.,), demonstrating the interplay of source altitude, beam tilt, and electric field model in fitting an individual spectrum. At 475 km, their event contained some harder photons (> 1 MeV) which may have been un-Comptonized or only forward-scattered. For our Event 3, at 747 km and with almost nothing above 1 MeV, there would be less ability to make constraints among these parameters, as we would likely be outside the unscattered cone of even a broadened or moderately tilted beam.**

Events 4 and 5 were chosen to represent the longest set of paralyzing events; Event 4 because it has the longest period of near-paralysis in the data set, and Event 5 because it is the only longer event that has a WWLLN flash match.

2.4 A new method for finding the luminosity of TGFs

Since RHESSI is paralyzed during the middle of Events 1, 2, 4, and 5, we cannot find their true intensity using conventional methods. We can, however, use the Compton tail to find the brightness of these TGFs, and of course we can also do this for Event 3, which is nothing but a Compton tail. Since most Compton-scattered photons have changed direction a few times on their way to the satellite, they have traveled a further distance than non-scattered photons and arrive later. Since during the Compton tail RHESSI is not paralyzed, we can use the tail to find the true brightness of the TGF.

The multiple Compton scatters nearly isotropize the delayed component, meaning that the angular distribution (beaming) of the original emission has virtually no impact on the derived estimate of the total luminosity. Figure 4 illustrates this effect. It is based on the first-stage GEANT3 simulations that propagate TGF photons from the source (in this case at 13 km) to spacecraft altitude. It shows the TGF luminosity you would deduce based on looking at the Compton scattered component (dashed lines) versus what you would deduce from all photons (solid lines) given the detection of a TGF with a total fluence of 0.1 photon/cm^2. At large radial distances (>300 km), both the narrowest beam allowed by the REAM simulation package and a broader beam give nearly identical results, since in both cases the Comptonized photons dominate. At smaller radii, however, where the majority of detected TGFs occur, using only the time-delayed, Comptonized tail allows the intrinsic luminosity to be reliably constrained regardless of the beam width, while using all the TGF photons does not. **For this example, the narrow beam is based on a uniform, vertical electric field and includes the broadening effects of both electron scattering and the natural angular distribution of bremsstrahlung relative to the electron's instantaneous direction (Dwyer, ,); for the broad beam, the gamma-rays before atmospheric Comptonization are started isotropicaly within a cone of 45 degrees half angle.**

This is an important development because angular distribution is the only parameter that currently cannot be measured. The other two parameters affecting luminosity estimates that are not available from the satellite gamma-ray data are the distance to the TGF and its production altitude. The former has long been available for some events by identifying the matching radio atmospheric (sferic), and the latter is becoming better and better understood based on detailed studies of radio waveforms (Stanley et al., , , , , e.g.).

2.5 Simulation procedure

To begin with, we model a TGF using the energy spectrum and angular distribution of photons calculated for an RREA by Dwyer () at three altitudes: 11 km, 13 km, and 15 km. Photons are propagated through the atmosphere using a realistic density model (Humphreys,) to the spacecraft altitude, 580 km, using GEANT3. The photons are then collected in rings based on the radial distance at spacecraft altitude from the point directly above the TGF. The radial ranges of the rings are chosen based on the known or hypothesized location of the TGF being modeled.

The collected photons in a given ring are then inserted into the mass model of RHESSI and its detectors, also using GEANT3. **For TGFs whose position is known, the photons are sent in in the appropriate direction corresponding to their point of origin; for Event 1, whose origin is unknown, they were sent into the spacecraft isotropically. Comparing isotropic and appropriately directed beams in the other events, we don't see a difference of more than ∼25% in the overall effective area of the instrument.** This simulation samples each output photon of the first simulation stage many times, but as these photons are each started at a random spot on the sphere containing the spacecraft mass model, and interact in different ways with the spacecraft and detectors, each output count in the second stage simulation is still unique. This second stage simulation is run until there is a population of several hundred thousand simulated events to choose from (an "event" may include more than one "hit" if the photon scattered between detector segments). Because each ring covers a range of possible spacecraft locations, when we really want to represent a single one, we correct the arrival time of each photon to be what it would be if it had originated at the center of the ring.

In the third and last stage of the simulation, we model the response of the detector electronics to a TGF whose counts are sampled from the large number of candidate events in the second-stage simulation. A desired number of counts (typically 100-1000 or so when modeling paralyzing TGFs) is randomly selected from the list of second-stage output events, and the arrival times at the spacecraft are convolved with a function of time (a Gaussian or square pulse) to represent the non-zero duration of the TGF. The electronics simulation includes the effects of deadtime, pileup and pileup rejection, and preamplifier resets, so it simulates the paralysis in the peak of the TGF. **The need to pay careful attention to instrumental deadtime in TGFs has been known for a while, but the importance of including the effects of pileup has become clearer more recently, particularly in the re-analysis of AGILE data by Marisaldi et al. (), which demonstrated that an apparent extra high-energy component in the spectrum could be explained by pileup and deadtime issues. Their procedure was similar to the multi-stage simulation outlined here.**

To constrain the luminosity range of a paralyzed TGF, we have essentially three observables: 1) the number of counts in the Compton tail; 2) the lack of in-scale counts during the period of paralysis (which sets a lower limit to the count rate); and 3) the fact that the rear segments do not all appear to go into reset together after the main peak, which would create a distinct gap of about 35μs between the paralyzed peak and the Compton tail (this constraint sets an upper limit to the count rate). **We can also use the number of counts that appear before paralysis begins to constrain the rise time of the TGF pulse, given constraints on its luminosity from the other parameters; see the analysis for Event 2 below.**

To set a luminosity lower limit for each TGF, we successively hypothesized that the TGF consisted, before the effects of the electronics, of a number N of individual photon events, with N allowed to vary over a wide range (e.g. from 50 to 1000). For each value of N, we took 5000 different random samples of N counts from the stage-two output file and ran the stage-three analysis to produce 5000 artificial TGFs. We then looked to see what fraction of these 5000 artificial TGFs gave greater than or equal to the true number of counts C in the Compton tail. The lowest value of N that gave $\geq C$ tail counts more than 5% of the time is our lower limit on N. By following the normalization carefully back through the three stages of the simulation, each value of N can be converted to a photon **fluence** at the spacecraft and to the total number of x/gamma-rays in the TGF > 20 keV (see Table 2). Again, since only the Comptonized photons are included, changing the beam width doesn't significantly change the results (see Figure 4).

Different authors have used different standards to define the luminosity of a TGF; the values for the lower limits on TGF luminosity in the right-hand columns of Table 2 can be converted as follows. To convert to photons > 1 MeV (as used by Bowers et al. ()), divide the number of photons > 20 keV by a factor of 5.41. This is a characteristic of the generic RREA spectrum (Dwyer, ,).

Dwyer et al. () proposed a standard measure of TGF source strength, Ξ, defined as the total grams per square centimeter of atmospheric column traversed by relativistic electrons during the event. This parameter is closely related to the number of gamma-rays produced, and the conversion from x/gamma-rays > 1 MeV to Ξ is given in that paper by $N_\gamma = \Xi/33.2$ g cm^{-2}; thus to convert from photons > 20 keV directly to Ξ, multiply the values in the last three columns of Table 2 by $(33.2/5.41) = 6.14$ g cm^{-2}. Dwyer et al. () defined a "standard TGF" as having $\Xi_0 = 10^{18}$ g cm^{-2}, and therefore Events 1, 2, 3, and 5, depending on their source altitude, are tens to hundreds of times as bright as this definition of an ordinary TGF.

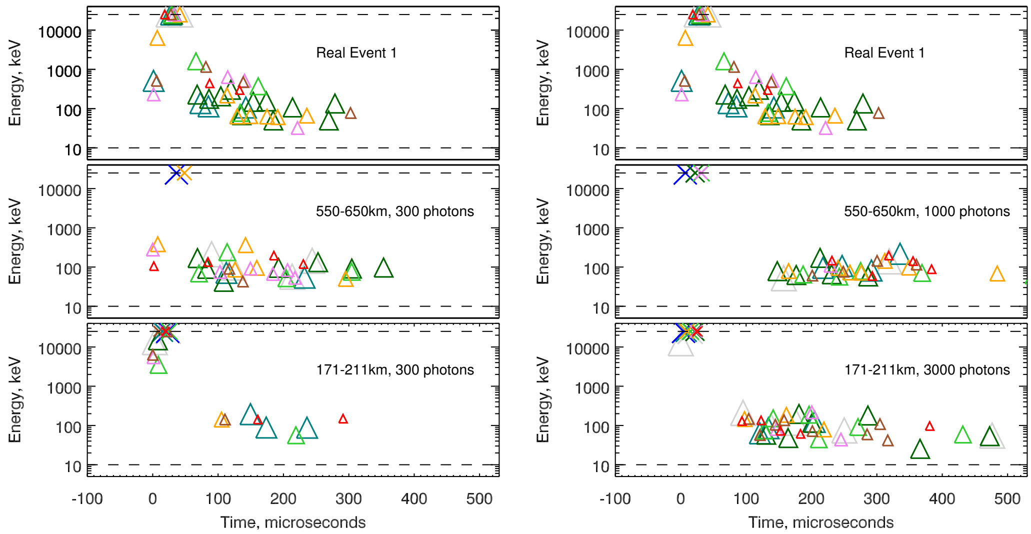

Figure 5. Top: the real Event 1 (repeated from Figure 1 and shown twice for easy of comparison with the simulations). Middle, left: simulation of a TGF that included 300 photon events before considering deadtime (13 km altitude, 550–650 km distance). Middle, right: the same but with 1000 photon events. Bottom, left: simulation at 13 km altitude, 171–211 km distance, 300 photon events. Bottom right: the same but with 3000 photon events.

Finally, the number of relativistic electrons in the avalanche has been used as a measure of luminosity by, e.g., Mailyan et al. () and Dwyer and Smith (). Unlike the number of gamma-rays or Ξ, however, the number of electrons corresponding to a given observed TGF is a strong function of the electric field assumed (Dwyer et al.,). For 400 kV/m sea level equivalent, as used by Mailyan et al. () and Dwyer and Smith (), the average relativistic electron passes through 11 g cm^{-2} (Dwyer et al.,), so our number of source photons > 20 keV can be multiplied by $(6.14 \text{ g cm}^{-2})/(11 \text{ g cm}^{-2}) = 0.56$ to give the number of relativistic avalanche electrons. The resulting values of 7.9 and 6.7 $\times 10^{18}$ relativistic electrons for Events 1 and 3 under the assumption of a 13 km altitude are comparable to the two most intrinsically luminous events shown by Mailyan et al. () in their Figure 8b for an assumed altitude of 13.6 km. One of these two events, like our Event 3, was very distant (666 km). It is not surprising that the brightest events will first be seen at large distances, since there is more geographical area at large radii and the instruments are still sensitive at those distance only for the brightest events.

2.6 Results on specific paralyzing TGFs

2.6.1 Event 1

This event, with the brightest Compton tail of any TGF we have examined, had no direct match with a WWLLN flash. Since the closest flash within half an hour was at 191 km, we first tried using the range 171–211 km to collect output counts from the stage one (atmospheric) simulation. When we continued the analysis through the final simulation stage, however, we found that it was impossible to get sufficient counts in the Compton tail without driving all the rear segments into reset during the TGF peak, which would create a gap between the paralyzed interval and the tail that isn't observed (see Figure 5, bottom panels). The resulting Compton tail also extended too far in time; this is because the earliest (and brightest) part of the Compton tail is suppressed by the paralyzed interval due to resets, and so the entire TGF must be made brighter so that the

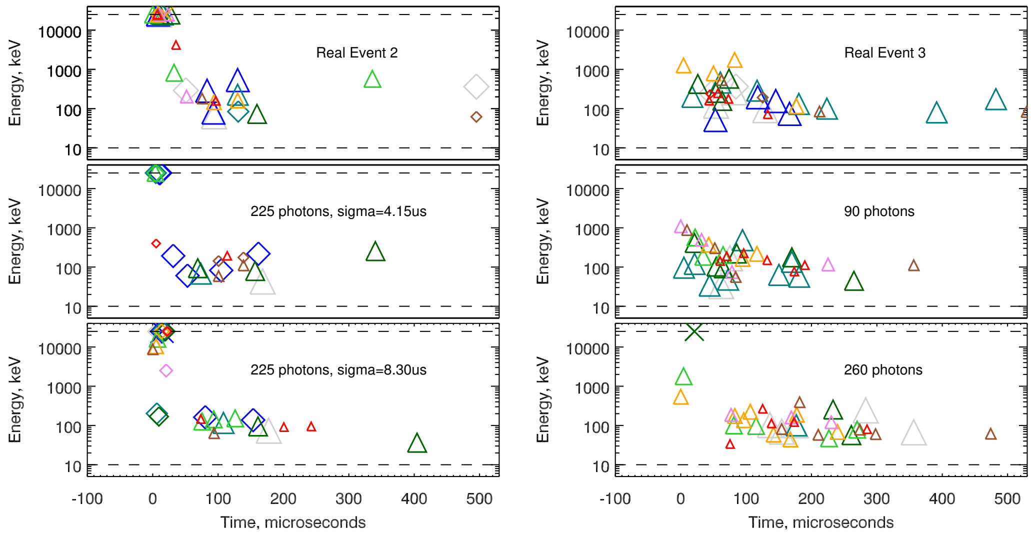

Figure 6. Top left: the real Event 2. Middle left: short risetime simulation (13 km, narrow beam, 234–294 km distance) that agrees well qualitatively with the real event. Bottom left: a longer risetime simulation showing a large number of counts before paralysis, which are not seen in this event. Top right: the real Event 3. Middle right: simulation with 90 photon events, 13 km altitude, narrow beam, 700-800 km distance. Bottom right: simulation with 260 photon events showing a similar number of recorded hits due to high deadtime earlier in the Compton tail.

later, fainter parts of the tail can be picked up in order to get the right total number of counts in the tail. These problems persisted even for the narrowest-beam simulations (using the native width of the beam from the REAM simulations with a parallel upward electric field).

The only way to reconcile the simulations to the data is to assume that the TGF occurred at a distance far enough away that the peak/tail ratio was much lower, but not so far away that the peak disappeared but only the tail remained (which is the case for Event 3). The middle row of panels in Figure 5 show simulations based on collecting the stage-one photons in a band from 550–650 km. At this range there are more Comptonized photons per peak photon, and the data can be reproduced well with roughly 300 photon events (Figure 5, middle left panel). This distance range contains two storm cells with multiple WWLLN flashes (shown in purple in the left-hand panel of Figure 3). At much higher numbers of photon events (Figure 5, middle right panel) we again reach the situation where there is high deadtime in the early part of the tail and the later parts of the tail start to appear, in disagreement with the data. The duration of the main (less Comptonized, paralyzing) TGF interval is short, and has been modeled in Figure 5 as a Gaussian with $\sigma = 10\mu$s. **This duration is not well constrained, and we have not attempted to constrain it in this analysis, but this value typically gives a comparable number of counts on the rise of the event before paralysis, and does not overlap the tail interval in the simulations, in qualitative agreement with the data.**

2.6.2 Event 2

For Events 2, 3, and 5 we know the storm cell responsible for the TGF from the WWLLN localization, and can estimate not only the distance to the TGF but its production altitude as well. We took the cloud top altitudes derived from infrared measurements and soundings (see Appendix) for these events and for the event of Lu et al. (), a TGF whose production altitude was constrained to 10–13 km by VHF data. Assuming a roughly constant distance between the IR cloud top altitude and the TGF production altitude, we thus estimated the TGF production altitude ranges of for Events 2, 3, and 5 given in Table 1. In Table 2, we have placed in parentheses the calculated lower limits on total TGF luminosity for the altitudes that we deem less likely using this method.

The notable feature of Event 2 is that there were no counts recorded before the moment that all of RHESSI's detectors went into paralysis. This implies a very fast risetime. The fastest risetime reported for a TGF was 7μs, by Foley et al. () in an event seen with Fermi. In our simulations of the response of the RHESSI electronics, we use a Gaussian shape for the original (unscattered) time profile. A risetime of 7μs from 10% to 90% intensity, as defined by Foley et al. (), corresponds to a Gaussian of $\sigma = 4.15\mu$s. When we simulate a TGF at the correct distance, with a narrow upward beam, we can replicate the absence of initial counts and the appearance of the Compton tail fairly well (Figure 6, middle left panel). For 225 photon events simulated before deadtime with this σ, 4.2% of the simulations show no count before paralysis, and 14% have at least as many counts in the Compton tail as the data for this event. Making the event even brighter improves both of these percentages but also makes it more likely that all the detectors go into reset in the main peak, producing a gap between the paralysis interval and the observed part of the Compton tail that isn't observed. If the TGF were even shorter, the probability of seeing no counts before paralysis would improve. But we do not take this as evidence of a risetime faster than that found by Foley et al. (). Event 2 was selected for presentation and analysis here exactly because it was one of only two events in our list that had no counts on the rise, and the only one with a WWLLN match.

As an example of what a slower rise would look like, we show in Figure 6, lower left panel, a simulation of the same sort but with $\sigma = 8.30\mu$s, twice as long. Only **0.06%** of such simulations show no count before paralysis sets in. Yet even this is an unusually short duration for a TGF (see, e.g., section 4 below). Due to the paralysis, we cannot constrain the fall time of the TGF as well as the risetime, in case it is asymmetrical, as is common in TGFs even excluding the fully Comptonized counts (Foley et al.,), but it must be less than about 50μs since only < 1 MeV, presumably Comptonized counts appear after the period of paralysis.

2.6.3 Event 3

While this event does not show a period of paralysis, what it shares with Events 1 and 2 is a very high derived luminosity. In this event, it appears that only the Compton tail is observed, consistent with simulations using a narrow TGF beam and the known distance from RHESSI's subsatellite point (747 km, with photons gathered from the simulation in the 700–800 km band). In the lower two panels on the right of Figure 6, we show two simulations that result in a comparable number of hits in the Compton tail (31 hits in the real event). In the center panel is a simulation with 90 photon events, and in the bottom is a simulation with 260 events. In the latter, there is such high deadtime early on that most of the counts are in later parts of the tail, in disagreement with the data, which looks more like the center panel. Simulations with much fewer than 90 photon events give too few hits in the tail due to deadtime.

2.6.4 Events 4 & 5

As can be seen in Table 2, the long period of paralysis of Event 5 implies the highest number of photons interacting in the detector of all the localized events, and the highest implied photon **fluence**; but this does not translate to a high intrinsic luminosity compared to the other events, since this event occurred almost immediately beneath the spacecraft, so that we have modeled RHESSI as being in the bright core of the TGF beam.

Table 2. 95% confidence lower limits for four paralyzing TGFs

	photons interacting			photon **fluence** (cm^{-2})			$\times 10^{17}$ photons > 20 keV		
Event	11 km	13 km	15 km	11 km	13 km	15 km	11 km	13 km	15 km
1	192	200	199	0.756	0.788	0.789	540	141	45
2	185	167	150	0.489	0.432	0.405	57	13	(4.0)
3	87	92	95	0.272	0.279	0.285	(353)	89	30
5	291	289	287	0.864	0.860	0.872	35	9.1	3.2

Figure 7 compares Event 5 with a typical simulation that reproduces its appearance fairly well; it consisted of 425 photons interacting with the detectors and had a Gaussian profile with $\sigma = 32\mu$s.

Because Event 4 is not localized, we don't know if this is the case for it as well, or whether it is offset by a couple of hundred kilometers and actually one of our brightest events.

Even though these two events are unusually long in their period of paralysis, they are not unusually long for TGFs; in fact, they are shorter than most members of the original population of RHESSI TGFs identified in the first RHESSI catalog (Grefenstette et al.,). The algorithm used to discover the paralyzing TGFs discussed in this section should have found any TGFs bright enough and long enough to have paralyzed the instrument for more than $200\mu s$ if they existed in RHESSI's data.

2.7 Paralyzing events and the TGF luminosity distribution

It is difficult to provide a clear answer to the question of whether the number of paralying TGFs in Figure 2 (40) is consistent with the expected power-law index of detected TGF counts, approximately -2.3 (Østgaard et al., , ,). A proper analysis would require not only further simulations to determine exactly how our algorithm to tag TGFs as paralyzing is sensitive to the TGF's duration, but also an understanding of how the duration distribution of TGFs varies with their luminosity. To forge ahead anyway with a crude estimate, we take the number of counts at which RHESSI catches 50% of TGFs at all to be 15 (see Figure A1 of Smith et al. ()), and the number of counts at which a TGF is likely to be tagged as paralyzing as 150 (see Table 2). The number of TGFs in the current catalog is 3249, and thus the derived index is $\log_{150/15}(40/3249) = -1.9$. **Considering all the uncertainties, we see no reason to claim that this is inconsistent with the paralyzed events being simply RHESSI's response to the shortest, brightest TGFs in the expected distribution.**

3 "Round trip" electron-beam events

As previously mentioned, terrestrial gamma-ray flashes emit secondary particle beams into space in addition to gamma-rays (Smith et al., , , , ,). Energetic electrons are created when TGF gamma-rays Compton scatter from electrons in air molecules high in the stratosphere, where they have enough energy to escape; pair production by gamma-rays on atomic nuclei adds an equal number of extra electrons and positrons to the beam. The particles in the beam undergo cyclotron motion and follow a field line of Earth's magnetic field into space, remaining relatively compact while the gamma-rays spread out geometrically. Thus, even though the total number of gamma-rays is much larger than the number of particles, by the time both populations reach low Earth orbit, the intensity

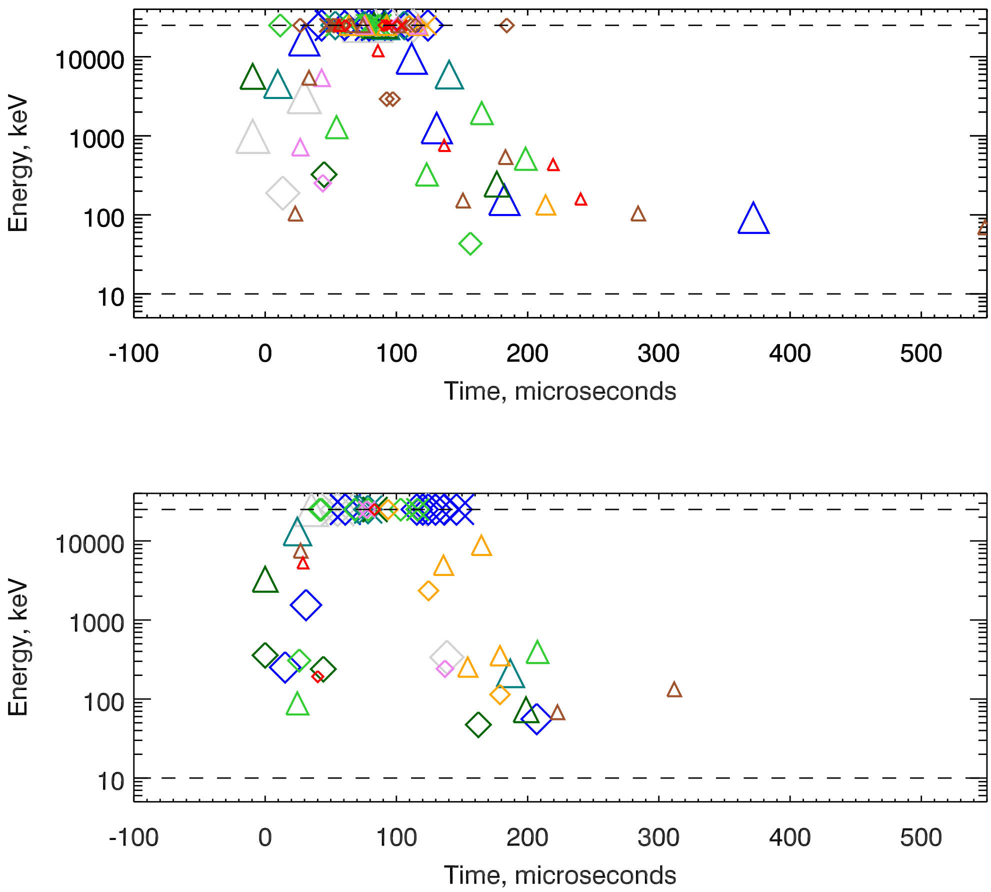

539 **Figure 7.** Top: the real Event 5. Bottom: simulation (425 interacting photons, duration
540 $\sigma = 32\mu$s, 13 km altitude, narrow beam, 110–150 km distance) that agrees well qualitatively with
541 the real event.

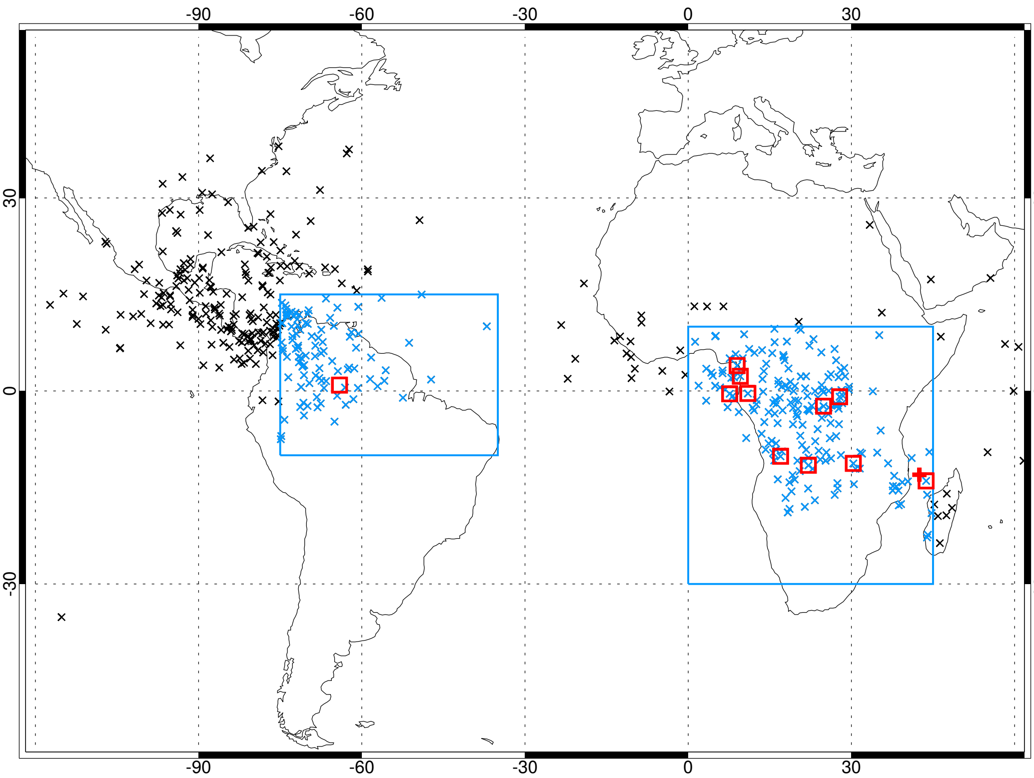

559 **Figure 8.** Geographic locations of the eleven candidate events for returning electron beams
560 (red boxes). The blue boxes show the boundary zones of the search and the blue crosses are all
561 the TGFs in these zones that did not meet the criteria for duration and brightness to be exam-
562 ined further.

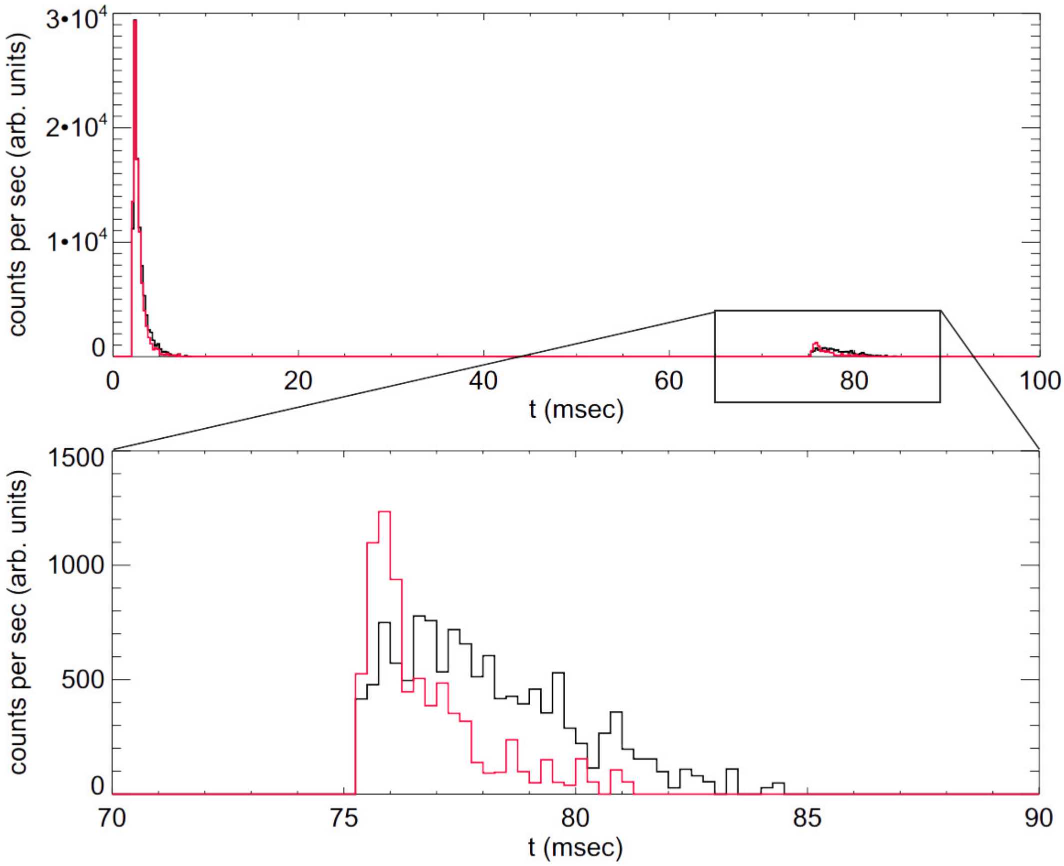

Figure 9. Simulation of the TGF/electron beam on February 12, 2005, with its return echo for all electrons (black) and electrons with energies ≥ 3 MeV (red). The zoom on the return pulse shows a tightening when only considering high energies.

of the particle beam can be somewhat higher than that of the gamma-ray beam, so that it can easily detected – although rare, since the area of the beam remains small (Carlson et al.,). The positron content of the beams has been spectacularly confirmed by observations with Fermi (Briggs et al.,).

If the magnetic field at the magnetic conjugate point is strong enough to reflect the particle beam, the beam can make both **an outward and a returning** pass through the spacecraft, losing only the particles nearly parallel to the magnetic field to the atmosphere in the interim. **This characteristic double pulse has been observed several times when the spacecraft was near the conjugate point and the two pulses merge together to a "double-horned" time profile (Smith et al., , , ,), and, as expected, this shape appears only in the cases where the magnetic field is indeed higher at the spacecraft position and the TGF is coming from the conjugate point.**

When the spacecraft is near the point of origin of the TGF and positioned in the outgoing electron beam, the returning beam from the conjugate point comes after a much longer interval. Only one previous case of an event in this geometry has been reported (Stanbro et al.,). Because a spacecraft in low-Earth orbit travels at about 7.5 km/s, and since the TGF particle beam is tens of kilometers across, the spacecraft is likely to still be in the beam after it has made a round trip to the magnetic conjugate point and returned. Stanbro et al. () saw three temporally distinct and significant features corresponding to the TGF gamma-rays, the electron beam on its way up (peaking about 1 ms later) and the electron beam returning from the conjugate hemisphere (about 89 ms later). Temporal **(Briggs et al.,), spectral (Briggs et al.,), and directional (Dwyer et al.,) analysis can help distinguish the direct gamma-ray beam from the upward electron beam, or even separate both components when visible (Sarria et al.,), but RHESSI, Fermi, and ASIM cannot intrinsically distinguish electrons from photons.**

3.1 Selection of events to search for the reflected beam

In order to identify electron beam events in RHESSI that have taken a round trip to and from the conjugate point, we first find geographical areas that have a weaker magnetic field relative to their conjugate point. Earth's magnetic field is weakest in South America and central Africa, so these regions will most clearly have a higher field at the conjugate point; however, much of the useful South American zone is in the South Atlantic Anomaly, where RHESSI's orbit passes through the inner radiation belt and data are not collected. Thus, the locations we searched were restricted to 10° S - 15° N and 75° W - 35° W for the northern coast of South America, and 30° S - 10° N and 0° E - 45° E for southern Africa. These zones are shown in Fig. 8.

We searched the first TGF catalog (Grefenstette et al.,) for events in these regions (one event in 2012 was added, although it was not in the original catalog, as it is clearly an electron beam.) We also restricted our search to events greater than 1 ms in duration. Electrons in an electron beam have a dispersion in time related to their pitch angle **(Dwyer et al.,)**. All the electrons of interest move nearly at the speed of light, so this is not a conventional velocity dispersion, but rather relates to how tight a **helix** they travel in; electrons with a smaller pitch angle will arrive slightly sooner than electrons with a larger angle **(see a nice illustration in Figure 1 of Sarria et al. ())**. Long events are not conclusively electron beams, but this eliminates shorter events which must be gamma-rays. We also restricted our search to events containing at least forty counts in the entire burst. Although these large events may or may not be more likely to be electron beams than dimmer events, they are certainly more likely to have a bright echo, should one exist.

Table 3. Candidate TGFs for a returning electron beam

TGF Timestamp	Latitude (°N)	Longitude (°E)	Duration (ms)	Counts	Separation (ms)
2002-10-18 16:40:14	-2.359	24.877	1.04	45	56
2003-02-23 19:54:07	-0.389	10.972	2.63	44	54
2003-03-23 17:57:01	-10.160	16.976	1.43	71	74
2003-05-17 18:47:01	3.947	9.000	2.93	67	47
2004-03-14 13:44:52	-11.558	22.086	1.53	40	77
2005-02-12 14:59:27	-11.260	30.349	1.81	65	74
2005-03-02 08:00:47	-0.909	27.828	1.02	60	53
2006-03-27 00:12:48	2.290	9.582	1.74	52	49
2007-03-05 22:22:42	-13.976	43.739	1.30	50	80
2007-12-05 06:32:02	-0.447	7.624	1.06	46	54
2012-10-27 22:44:26	0.910	295.905	1.23	82	12

After applying these filters on location, duration, and counts, the events listed in Table 3 remained.

3.2 Simulations

The events listed in Table 3 were modeled by the same code formerly used to generate electron beams self-consistently from TGF gamma rays and propagate them through Earth's magnetic field to the conjugate point (Dwyer et al.,). For this work, we make use only of one parameter from this simulation: the time delay between the initial TGF and the arrival of the electrons returning from the conjugate point. The field model used for this simulation was The International Association of Geomagnetism and Aeronomy (IAGA) 10th Generation International Geomagnetic Reference Field (`http://www.ngdc.noaa.gov/IAGA/vmod/igrf.html`).

A graphical example of the results of the simulation for the TGF on February 12, 2005 can be seen in Fig. 9. Table 3 also shows the simulated return time Δt of the electron beam relative to the initial burst, under "Separation". We pay particular attention to the high-energy electrons (> 3 MeV, shown in red in the figure) since they can penetrate RHESSI's aluminum cryostat and enter the detectors directly, giving a much higher detection probability than lower-energy electrons, which are seen only via their production of bremsstrahlung in the cryostat. The higher-energy electrons are also much more efficient bremsstrahlung producers and contribute more to the signal for that reason as well. The high-energy-only population has a sharper return signal because nearly all the dispersion is due to pitch-angle differences rather than velocity, which is nearly the speed of light for all electrons in the high energy band.

3.3 Analysis and results

After simulating the duration Δt between the electron beam and its echo, we created a histogram of each TGF's gamma-ray time profile with a bin size of 1 ms. We stacked the histograms by summing the histograms for all eleven events, with the timing aligned at the calculated return of the echo. The stacked histogram can be seen in Fig. 10. At $\Delta t = 0$, the exact point of alignment, a peak is visible. This peak contains 52 counts in one millisecond, compared to the stacked background of 25.98 counts per millisecond. This background was determined from the histogram following the point of alignment, to eliminate the contribution of the TGFs to the background. The Poisson probability of detecting at least this number of counts by chance is 4.53×10^{-6} (equivalent to 5.1σ significance for a normal distribution). The large peaks before $\Delta t = 0$ in the figure are

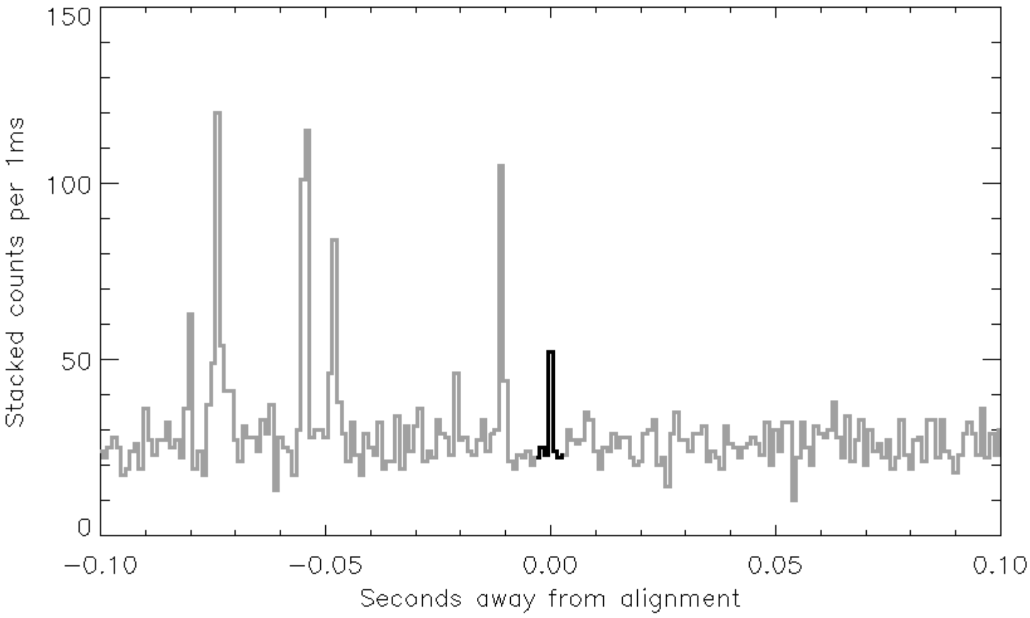

Figure 10. A stacked histogram of the electron beam candidate events, aligned at their simulated echo return. The peak at $\Delta t = 0$ (dark black) has a significance of 5.1σ. The peaks to the left of the plot are the individual triggered TGFs themselves, which are not aligned since the alignment is on the expected return time.

the original TGFs themselves. They are spread over a large range of times because of the different magnetic geometries in each case; to first order, the events that take place at higher magnetic latitude have a longer round trip to make and a greater temporal separation.

Table 4 shows the contribution of each TGF to this signal, along with its individual chance probability. The event on 2004-03-14 was a double-peaked event, and the initial peak was selected for the alignment to predict the return time; the others were all single-peaked and there was no such ambiguity. We find that five events in particular, listed first in the table, contributed significantly to this peak. Figure 8 on page 18 shows the geographic location of the eleven events.

3.4 Discussion

Nearly half of the events deemed most likely to include a returning electron beam did, indeed, do so. Naively, this might be surprising, since the radius at which the gamma-ray signal of a TGF can be detected (about 500 km, see e.g. Smith et al. ()) is much greater than the size of the electron beam (Carlson et al.,), and since we made no effort to pick TGFs where radio signals localized the origin to a spot near the satellite's magnetic footpoint. However, since we focused on longer-duration events, we suggest that most – or even all – of the longer TGFs identified by all spacecraft (1 ms or more in duration) may include the upward-going electron beam. This would include the great majority of the TGFs originally discovered by BATSE (Fishman et al.,), since BATSE's triggering algorithm was not sensitive to short events. **Briggs et al. () suggested that the two longest-duration TGFs in the early Fermi sample were upward electron beams based on their time profiles and soft spectra, and Briggs et al. () found a conclusive particle-beam signature in the presence of a bright positron-annihilation**

TGF Date	Counts at return	Background	Poisson Prob.
2007-12-05	9	2.94	0.0034
2006-03-27	9	3.19	0.0056
2004-03-14	7	2.35	0.020
2005-03-02	7	2.48	0.014
2005-02-12	6	2.80	0.065
2003-02-23	3	1.66	0.23
2003-05-17	4	2.96	0.35
2002-10-18	3	2.49	0.45
2007-03-05	1	1.19	0.70
2012-10-27	1	1.32	0.73
2003-03-23	2	2.62	0.74

Table 4. The contribution of each event to the electron beam return signal, along with their individual probabilities. The events which contributed most significantly are listed first.

line. Unfortunately, the summed spectrum of the first five TGFs in Table 4 has insufficient counts to determine if there is an unusual amount of positron annihilation.

The question **of whether there are any TGFs of relatively long duration that do *not* include a particle-beam contribution** can best be pursued by ASIM, TARANIS, and other upcoming missions that have the potential to separate electron and gamma-ray signals.

4 Geographic distribution of short TGFs

Both the first RHESSI TGF catalog (Grefenstette et al.,) and the second, which was developed at the University of Bergen (Gjesteland et al.,) analyzed the count rates in 1 ms bins to look for excesses indicating a TGF. This expectation was established by the BATSE observations (Fishman et al.,), but BATSE was insensitive to shorter events due to its onboard 64 ms integration window and high typical deadtime during TGFs (Grefenstette et al.,).

We therefore determined to re-analyze much of the RHESSI raw data using an algorithm that repeated the search for significant excesses using a range of time binnings: 60, 100, and 300μs, and 1, 3, 10, and 30 ms (the latter coarse binnings meant to enhance the sensitivity to electron beam events). Few new electron beam candidates were found, but we identified a large population of shorter TGFs in the 60μs and 100μs searches that had not been statistically significant when observed with 1 ms of background. Like the short TGFs found by Connaughton et al. () in Fermi data, these short events were more likely to match with radio signals from the World Wide Lightning Location Network (WWLLN) than longer events. In the analysis below, we also show that they are more likely to originate in the open ocean.

4.1 Search algorithm

The first catalog (Grefenstette et al.,) was very conservative, emphasizing confidence in each trigger over completeness, and we believe it contains few if any false positives. The newer algorithm more than doubles the rate of RHESSI TGF detection relative to the first catalog. In addition to adding the new search timescales, we followed Gjesteland et al. () in improving on the first catalog's algorithm by using true Poisson probabilities to make the cut on the likelihood of a given event being a chance coincidence. **The events used below have a probability of $< 2\times10^{-13}$ of being a chance collection of counts considering Poisson statistics alone.**

Using the early years of the mission as a baseline for comparison, through the end of 2007 the new algorithm (with the parameter settings used for this paper) gives 2057 TGFs, versus 812 in the first catalog and 1751 in the catalog of Gjesteland et al. (). The new catalog also shows very few events spread along the $\pm38^o$ lines of latitude, which is where the spacecraft spent the most time, since this was its orbital inclination. These events are a good diagnostic of when a large number of false events (statistical fluctuations) are contaminating the catalog. This effect can be seen in Figure 16 of Grefenstette et al. (), which was based on an earlier, less successful version of the algorithm currently in use. At `http://scipp.pbsci.ucsc.edu/rhessi/` users can compare, map, and download the events from the new algorithm, the first catalog algorithm, and the second catalog (Gjesteland et al.,) algorithm. The current database extends from the start of the mission to 30 November 2013 for the first catalog algorithm and the new algorithm, and to 10 September 2012 for the second catalog algorithm. RHESSI was still detecting TGFs after these dates, but the detector efficiency continued to decline due to radiation damage – see Albrechtsen et al. ().

The values of all the parameters used to generate the version of the catalog used in this paper are archived at `https://research-archive.scipp.ucsc.edu/rhessi_special` along with the catalog data. From time to time we will improve the algorithm and extend it to later dates in the mission history. When we do so, all such changes will be described, with their date, at the live site (`http://scipp.pbsci.ucsc.edu/rhessi/`).

4.2 Comparing short and long events

Many of the new events are short compared to those in the former catalogs, due to the new trigger timescales below 1 ms. Regardless of the time binning (or multiple binnings) in which a given event was triggered as significant, we define its length by the parameter "T68", the shortest time interval that contains 68% of the TGF counts. The number of background counts accidentally included within a millisecond is unlikely to be more than one, so most algorithms that decide which counts belong to the TGF, in order to decide what 68% of that number is, will come to approximately the same conclusion. To define clearly separated populations of long and short events for contrast, we define a short event – most of which come from the new search – as having T68 $<$ 50μs, and a long event as having T68 $>$ 100μs. There are 500 of the short events and 1592 of the long events, out of a total catalog population of 3249 events. **The histogram of all event durations (T68) is shown in Figure 11. For the longer values of T68, the distribution is approximated well by a power law of index -2.5, shown as a dashed line in the Figure. Some of the TGFs with T68 near or greater than 1 ms are double-peaked or electron-beam events. In Smith et al. () we demonstrated that there cannot be a much larger population of short TGFs that are being missed by our triggering algorithm, by stacking the gamma-ray signals in RHESSI at the times that the spacecraft was flying over lightning identified by WWLLN. Thus the turnover of the distribution below 100μs is neither entirely nor mostly an instrumental effect. Maps of the short and long populations are shown in the top panel of Figure 12.**

To search without preconception for differences in the geographical distribution of short and long events, we introduced a grid of circles of 1000 km radius on the Earth, with their centers spaced by 5^o in latitude and longitude (these circles overlap considerably). Within each circle, we calculate the binomial probability of getting either greater than or equal to, or less than or equal to, the number of short TGFs seen in that circle given the total number of TGFs it contains in the short plus long categories, with the

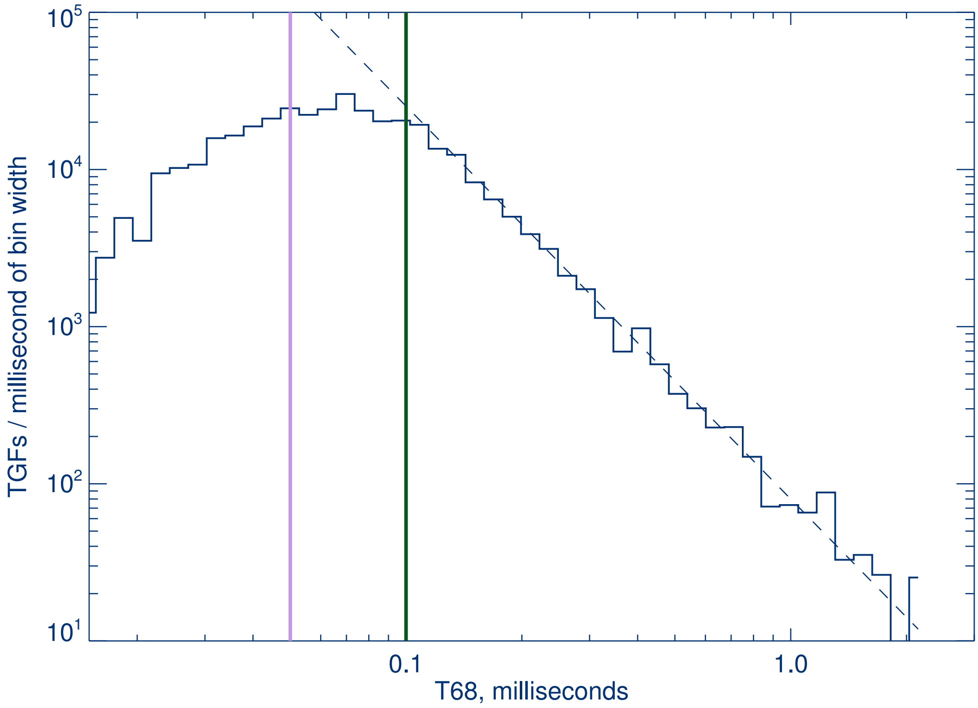

Figure 11. Histogram of the durations (T68) of 3249 RHESSI TGFs. The y axis is the density function (number of TGFs in the bin divided by the bin width) A power-law with index -2.5 is shown as a dashed line for comparison. The pink line shows the maximum T68 for the population we define as short, and the green line shows the minimum T68 for the population we define as long.

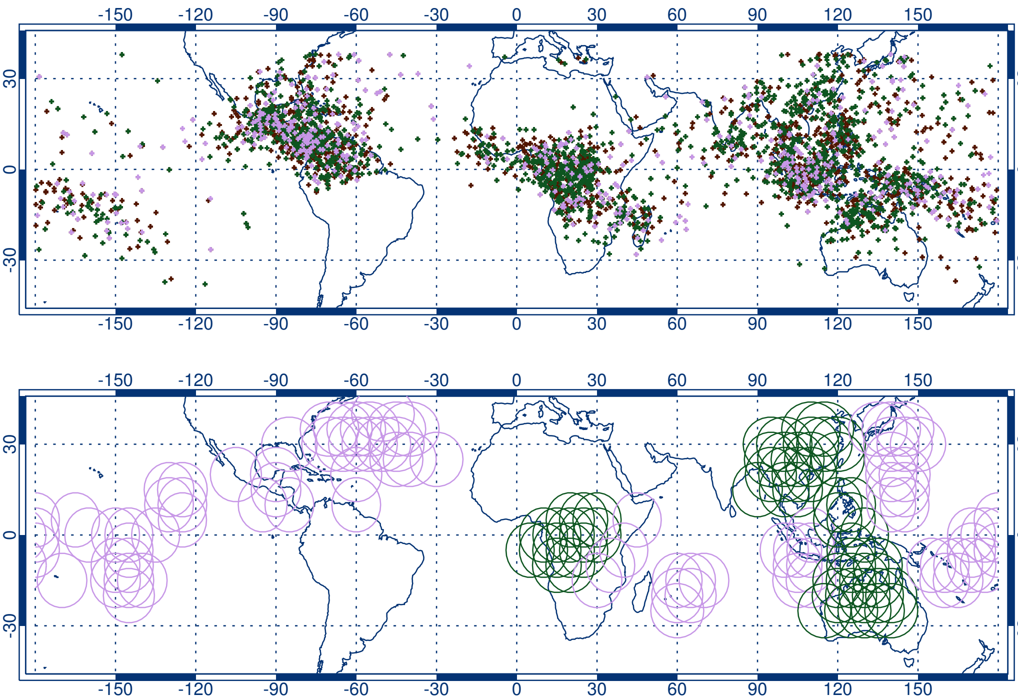

748 **Figure 12.** Top: RHESSI TGFs through 30 November 2013 using the new algorithm. Events
749 marked in pink have a T68 duration of $<$ 50μs and events marked in dark green have T68
750 $>$ 100μs. Bottom: regions with a binomial probability of $<$ 5% of having as high a fraction (pink)
751 or as low a fraction (green) by chance of $<$ 50μs TGFs as they do.

expectation probability calculated from the whole map (500 short TGFs out of 2092, or 23.9%). If this probability (in either direction) is less than 5%, the circle is plotted in color (pink for a larger than expected number of short events, dark green for a smaller). Circles with no TGFs, and circles with two or fewer, are naturally excluded – with only two TGFs in the circle, any combination of short and long durations has more than a 5% probability.

4.3 Discussion

Figure 12 shows that short events are consistently overabundant over oceans and underabundant over land. Even within the first catalog (Grefenstette et al.,) it was noted that TGFs over central Africa, the largest landlocked population, had an average duration longer than TGFs elsewhere in the world. Considering that many RHESSI TGFs suffer from deadtime, which suppresses counts in the event peak and would therefore increase T68, an alternate explanation for this effect could be that TGFs over central Africa are brighter. However, Fabró, Montanyà, van der Velde, Pineda, and Williams () have recently proposed that TGFs in this region might be underabundant relative to lightning (Smith et al.,) because strong updrafts compress the region between the main negative and upper positive charge centers of the storm, reducing the overall potential available for TGF avalanche multiplication and/or feedback. We expect that this scenario would be more likely to produce weak TGFs than unusually strong ones.

Roberts et al. () compared the duration distributions of Fermi TGFs over ocean and land and found no significant difference. Because of the many differences between our analyses, we do not claim that the two results are in conflict. In many of the oceanic regions where we find a significant excess of short TGFs, the *total* number of TGFs is rather small. Thus, if the numerous coastal TGFs have a duration distribution more similar to TGFs over land than to those over deep ocean, they might dilute an "oceanic" sample in a way that masks the duration effect of true deep-ocean TGFs, depending on the details of how coastal TGFs are classified as "land" or "ocean".

Connaughton et al. () noted that short TGFs are more powerful VLF emitters than other TGFs, matching sferic detections from WWLLN more often than longer TGFs, and, indeed, more often than either intracloud or cloud-to-ground lightning. This was attributed to the radio signal coming from current produced in the wake of the electron avalanches themselves, as opposed to the lightning channel (Cummer et al.,). The same effect appears when comparing the short and long events in RHESSI as well. The WWLLN flash match rate is 24.5% for the T68$< 50\mu$s sample, 9.2% for the T68$> 100\mu$s sample, and 15.8% for the whole catalog. These percentages use the TGFs from August 2003 onwards, for which WWLLN data are available. The efficiency of the WWLLN network was growing rapidly during the early years of the data set, but this doesn't affect the contrast between the different duration categories. For example, if the data set is restricted to January 2008 and onwards, all three WWLLN match rates go up as expected, but their relative differences are comparable, with 26.9%, 11.6%, and 19.8% match rates for the short, long, and full samples, respectively.

Under the feedback model of TGFs (Dwyer, ,), the full luminosity of a TGF is built up by having each relativistic avalanche produce more than one "daughter" avalanche. The total luminosity builds up exponentially as the total number of avalanches increases with each iteration of feedback, until the total currents produced by this process start to bring the electric field below the threshold for feedback. Short, bright TGFs in this model would be associated with high thundercloud potentials **and more avalanches produced in each "generation" of feedback**. This appears consistent with the trend of lower flash rates and higher peak currents for oceanic lightning in general, and the deficit

Event	IR Bright Merge (K)	IR Temp. °C	Sounding used	Est. Alt. (km)
Lu	214.0	-59.15	BNA 12Z	14.6
2	213.2	-59.15	TBPB Grantley 12Z	14.9
3	188.1	-85.05	moist model[a]	17.6
5	198.0	-75.15	YPDN 12Z	16.7

Table A.1. Data for cloudtop altitude calculations

[a] See text

of short TGFs over Africa appears consistent with the suggestion of Fabró et al. () of smaller potentials there due to the compression of the charge structure by strong updrafts.

Acknowledgments

The authors wish to thank the World Wide Lightning Location Network (`http://wwlln.net`), a collaboration among over 50 universities and institutions, for providing the lightning location data used in this paper. We also thank Thomas Gjesteland and Nikolai Ostgaard for making the second catalog data available.

Raw RHESSI data for the entire mission are available at `http://hesperia.gsfc.nasa.gov/hessidata/` or `http://soleil.i4ds.ch/hessidata/` but are best accessed by the automatic operation of the *Solarsoft* package of IDL routines, available at `http://www.lmsal.com/solarsoft/`. The original RHESSI TGF database of Grefenstette et al. () is available at `http://scipp.ucsc.edu/~dsmith/tgflib_public/`, although it doesn't contain all the events discussed in this paper. The most complete and current experimental database of RHESSI TGFs is at `http://scipp.pbsci.ucsc.edu/rhessi/` and allows a considerable amount of interactive exploration. A package of the software and reduced data sets creating the plots shown in this paper is hosted at `https://research-archive.scipp.ucsc.edu/rhessi_special`.

This work was supported by a grant from the National Science Foundation, ATM-0607885.

A Appendix: Estimation of cloud-top altitudes

Raw radiosonde data were obtained from the University of Wyoming's online data archive (`http://weather.uwyo.edu/upperair/sounding.html`) for times and locations nearest to the TGF event. Analysis of the radiosonde data was conducted using the MetPy package (May et al.,) and included estimates of the projected path (highlighted with the thick black curve on the Skew-T plots shown in Figure A.1) of a theoretical surface parcel of air lifted until saturated at the lifting condensation level (LCL) and then upwards from the LCL following moist-adiabatic ascent.

Temperatures from a globally-merged 4-km pixel-resolution IR satellite brightness temperature product (Janowiak et al.,) (Table A.1, first column) were used to estimate cloud top temperature (second column) for each case. The cloud top temperatures were than matched to an altitude in two ways (if possible). First, the cloud top temperature was simply matched to the first altitude reporting that temperature (gray shaded circle on the temperature curve) in the radiosonde temperature profile. Second, the cloud top temperature was matched to the first altitude reporting that temperature along the theoretical parcel path (green shaded circle on the parcel curve).

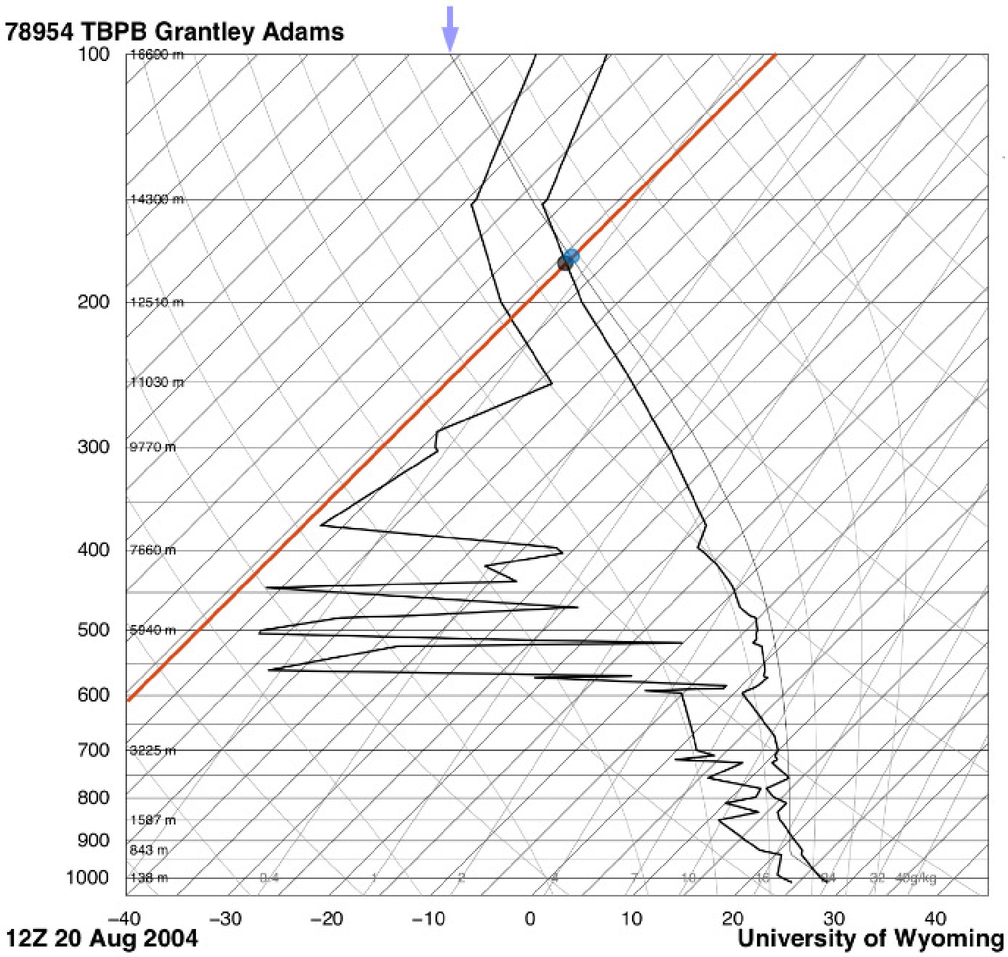

Figure A.1. Skew T-log p diagram of a proximity sounding for Event #2 from Grantley Adams International Airport (TBPB), Barbados, at 1200 UTC 20 Aug 2004. The black curves represent the observed temperature (right) and dew point (more jagged curve to the left). The curve marked with an arrow at the top represents a theoretical air parcel path lifted from the surface. The red line represents an estimate of observed cloud top temperature and the intersection between this line and the observed temperature and theoretical parcel path are denoted with black and green filled circles, respectively.

References

Albrechtsen, K. H., Østgaard, N., Berge, N., Gjesteland , T. (2019, Jan). Observationally Weak TGFs in the RHESSI Data. *Journal of Geophysical Research (Atmospheres)*, *124*(1), 287-298. doi: 10.1029/2018JD029272

Babich, L. P., Donskoy, E. N., Kutsyk, I. M. (2008, July). Analysis of atmospheric gamma-ray flashes detected in near space with allowance for the transport of photons in the atmosphere. *Soviet Journal of Experimental and Theoretical Physics*, *107*, 49-60. doi: 10.1134/S1063776108070042

Bowers, G. S., Smith, D. M., Kelley, N. A., Martinez-McKinney, G. F., Cummer, S. A., Dwyer, J. R., … Rassoul, H. K. (2018, May). A Terrestrial Gamma-Ray Flash inside the Eyewall of Hurricane Patricia. *Journal of Geophysical Research (Atmospheres)*, *123*, 4977-4987. doi: 10.1029/2017JD027771

Briggs, M. S., Connaughton, V., Wilson-Hodge, C., Preece, R. D., Fishman, G. J., Kippen, R. M., … Smith, D. M. (2011, January). Electron-positron beams from terrestrial lightning observed with Fermi GBM. *Geophys. Res. Let.*, *38*, L02808. doi: 10.1029/2010GL046259

Briggs, M. S., Fishman, G. J., Connaughton, V., Bhat, P. N., Paciesas, W. S., Preece, R. D., … Chekhtman, A. (2010). First results on terrestrial gamma ray flashes from the Fermi Gamma-ray Burst Monitor. *J. Geophys. Res.*, *115*, A07323. doi: 10.1029/2009JA015242

Carlson, B. E., Gjesteland, T., Østgaard, N. (2011, Nov). Terrestrial gamma-ray flash electron beam geometry, fluence, and detection frequency. *Journal of Geophysical Research (Space Physics)*, *116*(A11), A11217. doi: 10.1029/2011JA016812

Carlson, B. E., Lehtinen, N. G., Inan, U. S. (2010, October). Terrestrial gamma ray flash production by active lightning leader channels. *Journal of Geophysical Research (Space Physics)*, *115*, 10324. doi: 10.1029/2010JA015647

Cecil, D. J., Buechler, D. E., Blakeslee, R. J. (2014, January). Gridded lightning climatology from TRMM-LIS and OTD: Dataset description. *Atmospheric Research*, *135*, 404-414. doi: 10.1016/j.atmosres.2012.06.028

Celestin, S., Pasko, V. P. (2011, March). Energy and fluxes of thermal runaway electrons produced by exponential growth of streamers during the stepping of lightning leaders and in transient luminous events. *Journal of Geophysical Research (Space Physics)*, *116*, 3315. doi: 10.1029/2010JA016260

Celestin, S., Pasko, V. P. (2012, January). Compton scattering effects on the duration of terrestrial gamma-ray flashes. *Geophys. Res. Let.*, *39*, 2802. doi: 10.1029/2011GL050342

Cohen, M. B., Inan, U. S., Said, R. K., Briggs, M. S., Fishman, G. J., Connaughton, V., Cummer, S. A. (2010, September). A lightning discharge producing a beam of relativistic electrons into space. *Geophys. Res. Let.*, *37*, L18806. doi: 10.1029/2010GL044481

Connaughton, V., Briggs, M. S., Xiong, S., Dwyer, J. R., Hutchins, M. L., Grove, J. E., … Wilson-Hodge, C. (2013, May). Radio signals from electron beams in terrestrial gamma ray flashes. *Journal of Geophysical Research (Space Physics)*, *118*, 2313-2320. doi: 10.1029/2012JA018288

Cummer, S. A., Briggs, M. S., Dwyer, J. R., Xiong, S., Connaughton, V., Fishman, G. J., … Solanki, R. (2014, December). The source altitude, electric current, and intrinsic brightness of terrestrial gamma ray flashes. *Geophys. Res. Let.*, *41*, 8586-8593. doi: 10.1002/2014GL062196

Cummer, S. A., Lu, G., Briggs, M. S., Connaughton, V., Xiong, S., Fishman, G. J., Dwyer, J. R. (2011, July). The lightning-TGF relationship on microsecond timescales. *Geophys. Res. Let.*, *38*, 14810. doi: 10.1029/2011GL048099

Dwyer, J. R. (2003). A fundamental limit on electric fields in air. *Geophys. Res. Let.*, *30*(20), 2055.

Dwyer, J. R. (2008). Source mechanisms of terrestrial gamma-ray flashes. *J. Geophys. Res.*, *113*, D10103. doi: 10.1029/2007JD009248

Dwyer, J. R. (2012, February). The relativistic feedback discharge model of terrestrial gamma ray flashes. *Journal of Geophysical Research (Space Physics)*, *117*, 2308. doi: 10.1029/2011JA017160

Dwyer, J. R., Grefenstette, B. W., Smith, D. M. (2008). High-energy electron beams launched into space by thunderstorms. *Geophys. Res. Let.*, *35*, L02815. doi: 10.1029/2007/GL032430

Dwyer, J. R., Liu, N., Eric Grove, J., Rassoul, H., Smith, D. M. (2017, August). Characterizing the source properties of terrestrial gamma ray flashes. *Journal of Geophysical Research (Space Physics)*, *122*, 8915-8932. doi: 10.1002/2017JA024141

Dwyer, J. R., Smith, D. M. (2005). A comparison between Monte Carlo simulations of runaway breakdown and terrestrial gamma-ray flash observations. *Geophys. Res. Let.*, *32*, L08811. doi: 10.1028/2005GL023848

Dwyer, J. R., Smith, D. M., Uman, M. A., Saleh, Z., Grefenstette, B., Hazelton, B., Rassoul, H. K. (2010). Estimation of the fluence of high-energy electron bursts produced by thunderclouds and the resulting radiation doses received in aircraft. *J. Geophys. Res.*, *115*, D09206. doi: 10.1029/2009JD012039

Fabró, F., Montanyà, J., van der Velde, O. A., Pineda, N., Williams, E. R. (2019). On the tgf/lightning ratio asymmetry. *Journal of Geophysical Research: Atmospheres*, *124*(12), 6518-6531. Retrieved from `https://agupubs.onlinelibrary.wiley.com/doi/abs/10.1029/2018JD030075` doi: 10.1029/2018JD030075

Fishman, G. J., Bhat, P. N., Mallozzi, R., Horack, J. M., Koshut, T., Kouveliotou, C., ... Christian, H. J. (1994). Discovery of intense gamma-ray flashes of atmospheric origin. *Science*, *264*, 1313-1316.

Fitzpatrick, G., Cramer, E., McBreen, S., Briggs, M. S., Foley, S., Tierney, D., ... von Kienlin, A. (2014, August). Compton scattering in terrestrial gamma-ray flashes detected with the Fermi gamma-ray burst monitor. *Phys. Rev. D*, *90*(4), 043008. doi: 10.1103/PhysRevD.90.043008

Foley, S., Fitzpatrick, G., Briggs, M. S., Connaughton, V., Tierney, D., McBreen, S., ... Wilson-Hodge, C. (2014, July). Pulse properties of terrestrial gamma-ray flashes detected by the Fermi Gamma-Ray Burst Monitor. *Journal of Geophysical Research (Space Physics)*, *119*, 5931-5942. doi: 10.1002/2014JA019805

Gjesteland, T., Østgaard, N., Collier, A. B., Carlson, B. E., Eyles, C., Smith, D. M. (2012, March). A new method reveals more TGFs in the RHESSI data. *Geophys. Res. Let.*, *39*, 5102. doi: 10.1029/2012GL050899

Gjesteland, T., Østgaard, N., Connell, P. H., Stadsnes, J., Fishman, G. J. (2010, May). Effects of dead time losses on terrestrial gamma ray flash measurements with the Burst and Transient Source Experiment. *Journal of Geophysical Research (Space Physics)*, *115*, 0. doi: 10.1029/2009JA014578

Gjesteland, T., Østgaard, N., Laviola, S., Miglietta, M. M., Arnone, E., Marisaldi, M., ... Montanya, J. (2015, December). Observation of intrinsically bright terrestrial gamma ray flashes from the Mediterranean basin. *Journal of Geophysical Research (Atmospheres)*, *120*(D9), 12. doi: 10.1002/2015JD023704

Grefenstette, B. W., Smith, D. M., Dwyer, J. R., Fishman, G. J. (2008). Time evolution of terrestrial gamma-ray flashes. *Geophys. Res. Let.*, *35*(6), L06802. doi: 10.1029/2007/GL200703229

Grefenstette, B. W., Smith, D. M., Hazelton, B. J., Lopez, L. I. (2009). First RHESSI terrestrial gamma-ray flash catalog. *J. Geophys. Res.*, *114*, A02314. doi: 10.1029/2008JA013721

Gurevich, A. V., Milikh, G. M., Roussel-Dupré, R. A. (1992). Runaway electron mechanism of air breakdown and preconditioning during a thunderstorm. *Physics Letters A*, *165*, 463.

Hazelton, B., Grefenstette, B., Smith, D., Dwyer, J., Shao, X.-M., Cummer, S., ... Holzworth, R. (2009). Spectral dependence of terrestrial gamma-ray flashes on source distance. *Geophys. Res. Let.*, *36*, L01108. doi: 10.1029/2008GL035906

Humphreys, W. (1964). *Physics of air, 3rd ed.* Dover Publications.

Janowiak, J., Joyce, B., Xie, P. (2017). NCEP/CPC L3 half hourly 4km global (60S - 60N) merged IR V1. Goddard Earth Sciences Data and Information Services Center (GES DISC). (Andrey Savtchenko,editor, `https://doi.org/10.5067/P4HZB9N27EKU`, accessed December 2019)

Landis, D. A., Cork, C. P., Madden, N. W., Goulding, F. S. (1982, February). Transistor Reset Preamplifier for High Rate High Resolution Spectroscopy. *IEEE Transactions on Nuclear Science*, *29*, 619-624. doi: 10.1109/TNS.1982.4335922

Lu, G., Blakeslee, R. J., Li, J., Smith, D. M., Shao, X.-M., McCaul, E. W., ... Cummer, S. A. (2010). Lightning mapping observation of a terrestrial gamma-ray flash. *Geophys. Res. Let.*, *37*, L11806. doi: 10.1029/2010GL043494

Mailyan, B. G., Briggs, M. S., Cramer, E. S., Fitzpatrick, G., Roberts, O. J., Stanbro, M., ... Dwyer, J. R. (2016, November). The spectroscopy of individual terrestrial gamma-ray flashes: Constraining the source properties. *Journal of Geophysical Research (Space Physics)*, *121*(A10), 11. doi: 10.1002/2016JA022702

Mailyan, B. G., Xu, W., Celestin, S., Briggs, M. S., Dwyer, J. R., Cramer, E. S., ... Stanbro, M. (2019). Analysis of individual terrestrial gamma-ray flashes with lightning leader models and fermi gamma-ray burst monitor data. *Journal of Geophysical Research: Space Physics*, *124*(8), 7170-7183. Retrieved from `https://agupubs.onlinelibrary.wiley.com/doi/abs/10.1029/2019JA026912` doi: 10.1029/2019JA026912

Marisaldi, M., Argan, A., Ursi, A., Gjesteland, T., Fuschino, F., Labanti, C., ... Trois, A. (n.d.). Enhanced detection of terrestrial gamma-ray flashes by agile. *Geophysical Research Letters*, *42*(21), 9481-9487. Retrieved from `https://agupubs.onlinelibrary.wiley.com/doi/abs/10.1002/2015GL066100` doi: 10.1002/2015GL066100

Marisaldi, M., Fuschino, F., Labanti, C., Galli, M., Longo, F., Del Monte, E., ... Salotti, L. (2010, March). Detection of terrestrial gamma ray flashes up to 40 MeV by the AGILE satellite. *Journal of Geophysical Research (Space Physics)*, *115*, 0. doi: 10.1029/2009JA014502

Marisaldi, M., Fuschino, F., Tavani, M., Dietrich, S., Price, C., Galli, M., ... Vercellone, S. (2014, February). Properties of terrestrial gamma ray flashes detected by AGILE MCAL below 30 MeV. *Journal of Geophysical Research (Space Physics)*, *119*, 1337-1355. doi: 10.1002/2013JA019301

Marisaldi, M., Galli, M., Labanti, C., ÃŸstgaard, N., Sarria, D., Cummer, S. A., ... Verrecchia, F. (2019). On the high-energy spectral component and fine time structure of terrestrial gamma ray flashes. *Journal of Geophysical Research: Atmospheres*, *124*(14), 7484-7497. Retrieved from `https://agupubs.onlinelibrary.wiley.com/doi/abs/10.1029/2019JD030554` doi: 10.1029/2019JD030554

May, R. M., Arms, S. C., Marsh, P., Bruning, E., Leeman, J. R. (2017). *MetPy: A Python package for meteorological data.* `https://doi.org/10.5065/D6WW7G29`. Unidata.

Moss, G. D., Pasko, V. P., Liu, N., Veronis, G. (2006). Monte carlo model for analysis of thermal runaway electrons in streamer tips in transient luminous events and streamer zones of lightning leaders. *J. Geophys. Res.*, *111*, A02307.

Nemiroff, R. J., Bonnell, J. T., Norris, J. P. (1997). Temporal and spectral characteristics of terrestrial gamma ray flashes. *J. Geophys. Res.*, *102*(A5), 9659-9665.

Østgaard, N., Albrecthsen, K. H., Gjesteland, T., Collier, A. (2015, December). A new population of terrestrial gamma-ray flashes in the RHESSI data. *Geophys. Res. Let.*, *42*, 10. doi: 10.1002/2015GL067064

Østgaard, N., Balling, J. E., Bjørnsen, T., Brauer, P., Budtz-Jørgensen, C., Bujwan, W., ... Eyles, C. (2019, Feb). The Modular X- and Gamma-Ray Sensor (MXGS) of the ASIM Payload on the International Space Station. *Space Science Reviews*, *215*(2), 23. doi: 10.1007/s11214-018-0573-7

Østgaard, N., Gjesteland, T., Hansen, R. S., Collier, A. B., Carlson, B. (2012, March). The true fluence distribution of terrestrial gamma flashes at satellite altitude. *Journal of Geophysical Research (Space Physics)*, *117*, 3327. doi: 10.1029/2011JA017365

Østgaard, N., Gjesteland, T., Stadnses, J., Connell, P. H., Carlson, B. (2008). Production altitude and time delays of the terrestrial gamma flashes: Revisiting the burst and transient source experiment spectra. *J. Geophys. Res.*, *113*. doi: 10.1029/2007JA012618

Østgaard, N., Neubert, T., Reglero, V., Ullaland, K., Yang, S., Genov, G., ... Alnussirat, S. (2019). First 10 months of tgf observations by asim. *Journal of Geophysical Research: Atmospheres*, *124*(24), 14024-14036. Retrieved from `https://agupubs.onlinelibrary.wiley.com/doi/abs/10.1029/2019JD031214` doi: 10.1029/2019JD031214

Roberts, O. J., Fitzpatrick, G., Stanbro, M., McBreen, S., Briggs, M. S., Holzworth, R. H., ... Mailyan, B. G. (2018). The first fermi-gbm terrestrial gamma ray flash catalog. *Journal of Geophysical Research: Space Physics*, *123*(5), 4381-4401. Retrieved from `https://agupubs.onlinelibrary.wiley.com/doi/abs/10.1029/2017JA024837` doi: 10.1029/2017JA024837

Sarria, D., Blelly, P. L., Briggs, M. S., Forme, F. (2016, May). Studying the time histogram of a terrestrial electron beam detected from the opposite hemisphere of its associated TGF. *Journal of Geophysical Research (Space Physics)*, *121*(5), 4698-4704. doi: 10.1002/2015JA021881

Sarria, D., Kochkin, P., ÃŸstgaard, N., Lehtinen, N., Mezentsev, A., Marisaldi, M., ... Eyles, C. (2019). The first terrestrial electron beam observed by the atmosphere-space interactions monitor. *Journal of Geophysical Research: Space Physics*, *124*(12), 10497-10511. Retrieved from `https://agupubs.onlinelibrary.wiley.com/doi/abs/10.1029/2019JA027071` doi: 10.1029/2019JA027071

Shao, X.-M., Hamlin, T. D., Smith, D. M. (2010). A closer examination of terrestrial gamma-ray flash-related lightning processes. *J. Geophys. Res.*, *115*, A00E30. doi: 10.1029/2009JA014835

Smith, D. M., Buzbee, P., Kelley, N. A., Infanger, A., Holzworth, R. H., Dwyer, J. R. (2016, October). The rarity of terrestrial gamma-ray flashes: 2. RHESSI stacking analysis. *Journal of Geophysical Research (Atmospheres)*, *121*, 11. doi: 10.1002/2016JD025395

Smith, D. M., Dwyer, J. R., Grefenstette, B. W., Hazelton, B. J., Yair, Y., Bor, J., ... Holzworth, R. H. (2007). Unusual RHESSI TGFs: electron beams and others. *Eos Trans. AGU, Fall Meet. Suppl.*, *88*(52), AE31A-0051.

Smith, D. M., Dwyer, J. R., Hazelton, B. J., Grefenstette, B. W., Martinez-McKinney, G. F. M., Zhang, Z. Y., ... Blakeslee, R. J. (2011). The rarity of terrestrial gamma-ray flashes. *Geophys. Res. Let.*, *38*, L08807. doi: 10.1029/2011GL046875

Smith, D. M., Grefenstette, B. W., Splitt, M., Lazarus, S. M., Rassoul, H. K., Coleman, L. M., ... Takahashi, Y. (2006, December). The Anomalous Terrestrial Gamma-ray Flash of 17 January 2004. *AGU Fall Meeting Abstracts*, AE31A-1040.

Smith, D. M., Hazelton, B. J., Grefenstette, B. W., Dwyer, J. R., Holzworth, R. J., Lay, E. H. (2010). Terrestrial gamma ray flashes correlated to storm phase and tropopause height. *J. Geophys. Res.*, *115*, A00E49. doi:

10.1029/2009JA014853

Smith, D. M., Lin, R. P., Turin, P., Curtis, D. W., Primbsch, J. H., Cambell, R., ... Schwartz, R. (2002). The RHESSI Spectrometer. *Solar Physics*, *210*, 33-60.

Smith, D. M., Lopez, L. I., Lin, R. P., Barrington-Leigh, C. P. (2005). Terrestrial gamma-ray flashes observed up to 20 MeV. *Science*, *307*, 1085-1088.

Splitt, M. E., Lazarus, S. M., Barnes, D., Dwyer, J. R., Rassoul, H. K., Smith, D. M., ... Grefenstette, B. W. (2010). Thunderstorm characteristics associated with RHESSI-identified terrestrial gamma-ray flashes. *J. Geophys. Res.*, *115*, A00E38. doi: 10.1029/2009JA014622

Stanbro, M., Briggs, M. S., Roberts, O. J., E., C., R., D. J., Holzworth, R. H., ... Xiong, S. L. (2019). A Fermi Gamma-ray Burst Monitor Event Observed as a Terrestrial Gamma-ray Flash and Terrestrial Electron Beam. *Journal of Geophysical Research (Space Physics)*. doi: 10.1029/2019JA026749

Stanley, M. A., Shao, X., Smith, D. M., Lopez, L., Pongratz, M., Harlin, J., ... Regan, A. (2006). A link between terrestrial gamma-ray flashes and intracloud lightning discharges. *Geophys. Res. Let.*, *33*, L06803. doi: 10.1029/20005GL025537

Tierney, D., Briggs, M. S., Fitzpatrick, G., Chaplin, V. L., Foley, S., McBreen, S., ... Wilson-Hodge, C. (2013, October). Fluence distribution of terrestrial gamma ray flashes observed by the Fermi Gamma-ray Burst Monitor. *Journal of Geophysical Research (Space Physics)*, *118*, 6644-6650. doi: 10.1002/jgra.50580